J|A|C|S ARTICLES

Published on Web 08/04/2010

Concerted Proton−Electron Transfer to Dioxygen in Water

Ophir Snir,[†] Yifeng Wang,[†] Mark E. Tuckerman,[§] Yurii V. Geletii,[‡] and Ira A. Weinstock*,[†]

Department of Chemistry, Ben Gurion University of the Negev, Beer Sheva 84105, Israel, Department of Chemistry, Emory University, Atlanta, Georgia 30322, and Department of Chemistry and Courant Institute of Mathematical Sciences, New York University, New York, New York 10003

Received May 20, 2010; E-mail: iraw@bgu.ac.il

Abstract: Concerted proton−electron transfer (CPET) is documented for the homogeneous reduction of O_2 to $HO_2^{\bullet}$ in water by the one-electron-reduced heteropolytungstate anion, α-$PW_{12}O_{40}^{4-}$ ($\mathbf{1}_{1e}$). At 0.01−0.3 M H^+, O_2 reduction occurs via outer-sphere electron transfer followed by proton transfer (ETPT, with rate constant k_{ET}). Between 0.30 and 1.9 M H^+, rates increase linearly with $[H^+]$ due to a parallel CPET pathway in which H^+ is now a reactant: $(1/2)k_{obs} = k_{ET} + k_{CPET}[H^+]$ ($k_{ET} = 1.2$ M^{-1} s^{-1}; $k_{CPET} = 0.8$ M^{-2} s^{-1}). Control experiments rule out preassociation between H^+ and $\mathbf{1}_{1e}$. Analysis of plausible rate expressions shows that the first-order dependence on $[H^+]$ is uniquely consistent with multisite CPET, and a deuterium kinetic isotope effect of 1.7 is observed. Reductions of O_2 by α-$SiW_{12}O_{40}^{5-}$ confirm theoretical predictions that CPET decreases in significance as ET becomes less endergonic. Marcus analysis, including the temperature dependence of $\Delta G°$, gives reorganization energies, $\lambda_{ET} = 41.5$ kcal mol^{-1} and $\lambda_{CPET} = 52.4$ kcal mol^{-1}. At 1.5 M H^+, ~75% of the ($\mathbf{1}_{1e}$,O_2) encounter pairs form within 6 Å of H^+ ions. This value (6 ± 1 Å) is the "reaction distance" for proton diffusion and probably close to that for CPET. Even so, the 70−200 ps lifetimes of the ($\mathbf{1}_{1e}$,O_2) pairs provide additional time for H^+ to diffuse closer to O_2. CPET is first-order in $[H^+]$ because k_e for "cage escape" from ($\mathbf{1}_{1e}$,O_2) pairs is much larger than k_{CPET}, such that the rate expression for CPET becomes $-(1/2)d[\mathbf{1}_{1e}]/dt = (k_d/k_e)k_{CPET}[\mathbf{1}_{1e}][O_2][H^+]$, where k_d is the rate constant for ($\mathbf{1}_{1e}$,O_2) pair formation. Overall, the findings suggest that the emergence of CPET, with hydronium ion as the proton donor, may prove a general feature of sufficiently endergonic reductions of dioxygen by otherwise "outer-sphere" complexes (or electrode reactions) at sufficiently low pH values in water.

Introduction

Dioxygen (O_2) in its triplet ground electronic state is relatively inert. Once activated, however, its reactions are complex and difficult to control. Hence, despite oxygen's abundance in nature and its promise for use in clean chemical processes, its primary use remains as an oxidant for the combustion of fossil fuels. This is in stark contrast to biological systems, where enzymes exert remarkable control over the activation of dioxygen and over the intermediates formed during its multistep reduction to water (eq 1).

$$O_2 + 4H^+ + 4e^- \rightarrow 2H_2O \qquad (1)$$

For these reasons, new information about fundamental mechanistic steps in the reduction of dioxygen,[1] and its reverse, the oxidation of water,[2] can provide a basis for ongoing advances in chemical biology[3] and is critical to the use of O_2 in new catalytic processes[1e,h,4] and sustainable-energy technologies.[5]

In both biological and chemical contexts, mechanistic questions often concern the nature of individual electron- and proton-transfer steps. For example, electron transfer (ET) from metal centers or organic functional groups can occur via inner- or outer-sphere mechanisms, and proton transfer (PT) can occur *after* electron transfer (an ETPT mechanism) or via single-step processes such as concerted proton−electron transfer (CPET) and hydrogen-atom ($H^{\bullet}$) transfer (HAT).

We recently established that, at pH values between 2 and 7, ET to O_2 by one-electron-reduced Keggin heteropolytungstate cluster anions occurs via outer-sphere electron transfer (ET and

[†] Ben Gurion University of the Negev.
[§] New York University.
[‡] Emory University.

(1) (a) Tolman, W. B.; Solomon, E. I. *Inorg. Chem.* **2010**, *49*, 3555–3556. (b) Gewirth, A. A.; Thorum, M. S. *Inorg. Chem.* **2010**, *49*, 3557–3566. (c) Smeets, P. J.; Woertink, J. S.; Sels, B. F.; Solomon, E. I.; Schoonheydt, R. A. *Inorg. Chem.* **2010**, *49*, 3573–3583. (d) Bakac, A. *Inorg. Chem.* **2010**, *49*, 3584–3593. (e) Neumann, R. *Inorg. Chem.* **2010**, *49*, 3594–3601. (f) Mukherjee, A.; Cranswick, M. A.; Chakrabarti, M.; Paine, T. K.; Fujisawa, K.; Münck, E.; Que, L., Jr. *Inorg. Chem.* **2010**, *49*, 3618–3628. (g) Halime, Z.; Kieber-Emmons, M. T.; Qayyum, M. F.; Mondal, B.; Gandhi, T.; Puiu, S. C.; Chufan, E. E.; Sarjeant, A. A. N.; Hodgson, K. O.; Hedman, B.; Solomon, E. I.; Karlin, K. D. *Inorg. Chem.* **2010**, *49*, 3629–3645. (h) Shook, R. L.; Borovik, A. S. *Inorg. Chem.* **2010**, *49*, 3646–3660. (i) Ashley, C. D.; Brinkley, D. W.; Roth, J. P. *Inorg. Chem.* **2010**, *49*, 3661–3675. (j) Zhang, C.; Fan, F.-R. F.; Bard, A. J. *J. Am. Chem. Soc.* **2009**, *131*, 177–181. (k) Shao, M.-H.; Liu, P.; Adzic, R. R. *J. Am. Chem. Soc.* **2006**, *128*, 7408–7409. (l) Kim, J.; Gewirth, A. A. *J. Phys. Chem. B* **2006**, *110*, 2565–2571. (m) Costentin, C.; Evans, D. H.; Robert, M.; Savéant, J.-M.; Singh, P. S. *J. Am. Chem. Soc.* **2005**, *127*, 12490–12491. (n) Li, X.; Gewirth, A. A. *J. Am. Chem. Soc.* **2005**, *127*, 5252–5260. (o) Anderson, A. B.; Albu, T. V. *J. Am. Chem. Soc.* **1999**, *121*, 11855–11863.

 10.1021/ja104392k

ETPT mechanisms).[6] This was done using an isostructural series of 1e$^-$-reduced anions, α-Keggin-$X^{n+}W_{12}O_{40}^{(9-n)-}$, whose charges increased from 4− to 5− to 6− as the central heteroatom, X^{n+}, was varied from P^{5+} to Si^{4+} to Al^{3+}.[6,7] At pH 7, O_2 is reduced by outer-sphere ET to give the superoxide radical anion ($O_2^{\bullet-}$). The pK_a of the protonated superoxide radical ($HO_2^{\bullet}$) is 4.7,[8] and at pH 2, $O_2^{\bullet-}$ is rapidly protonated (an ETPT mechanism).

Now, using the one-electron-reduced heteropolyanion, α-$P^VW_{12}O_{40}^{4-}$ (**1**$_{1e}$, Figure 1), we document the emergence *at lower pH values* of a concerted (simultaneous) multisite proton−electron transfer[1m,o,9,10] pathway that converts O_2 directly to $HO_2^{\bullet}$ in a single elementary step.

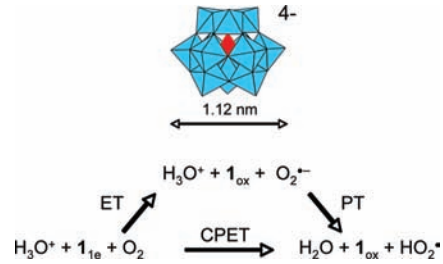

Figure 1. One-electron-reduced α-Keggin heteropolytungstate anion, α-$P^VW_{12}O_{40}^{4-}$ (**1**$_{1e}$, top), and its reactions with O_2 to give $HO_2^{\bullet}$ via ETPT and multisite CPET pathways. The cluster anion possesses tetrahedral (T_d) symmetry and contains 12 equivalent W atoms located at the center of 12 WO_6 polyhedra (shown in blue). At the center of the cluster (in red) is a tetrahedral PO_4^{3-} oxoanion.

In this multisite CPET,[11,12] the proton is supplied by a hydronium cation from bulk water (aq HCl), and the electron is donated by a freely diffusing molecular anion, **1**$_{1e}$. Unlike the electrochemical reduction of hydrogen-bonded superoxide complexes, $[(O_2^{\bullet-})(H_2O)]$, in organic solvents,[1m,13] the herein reported CPET reaction occurs in pure water, involves the first one-electron reduction of O_2 (i.e., the activation of dioxygen),[14] and is a *multisite process* involving ET from **1**$_{1e}$ to O_2 and PT from hydronium ion in bulk water. Moreover, the *directions* of PT and ET are the reverse of those in numerous CPET oxidations of tyrosine (TyrOH)[10c,15] and other phenols.[10a,b,16] In those cases, electrons travel from organic electron donors to metal complexes or electrodes, while protons are simultaneously *released* to pendant functional groups such as amines, to buffer anions,[15b,17] or to bulk water.[10c,15c−e,18]

(2) (a) Chen, Z.; Concepcion, J. J.; Hub, X.; Yang, W.; Hoertz, P. G.; Meyer, T. J. *Proc. Nat. Acad. Sci. U.S.A.* **2010**, *107*, 7225–7229. (b) Yin, Q.; Tan, J. M.; Besson, C.; Geletii, Y. V.; Musaev, D. G.; Kuznetsov, A. E.; Luo, Z.; Hardcastle, K. I.; Hill, C. L. *Science* **2010**, *328*, 342–345. (c) Geletii, Y. V.; Besson, C.; Hou, Y.; Yin, Q.; Musaev, D. G.; Quiñonero, D.; Cao, R.; Hardcastle, K. I.; Proust, A.; Kögerler, P.; Hill, C. L. *J. Am. Chem. Soc.* **2009**, *131*, 17360–17370. (d) Sala, X.; Romero, I.; Rodríguez, M.; Lluís, E.; Llobet, A. *Angew. Chem., Int. Ed.* **2009**, *48*, 2–13. (e) Youngblood, W. J.; Anna Lee, S.-H.; Kobayashi, Y.; Hernandez-Pagan, E. A.; Hoertz, P. G.; Moore, T. A.; Moore, A. L.; Gust, D.; Mallouk, T. E. *J. Am. Chem. Soc.* **2009**, *131*, 926–927. (f) Sartorel, A.; Carraro, M.; Scorrano, G.; De Zorzi, R.; Geremia, S.; McDaniel, N. D.; Bernhard, S.; Bonchio, M. *J. Am. Chem. Soc.* **2008**, *130*, 5006–5007. (g) Kanan, M. W.; Nocera, D. G. *Science* **2008**, *321*, 1072–1075. (h) Howells, A. R.; Sankarraj, A.; Shannon, C. *J. Am. Chem. Soc.* **2004**, *126*, 12258–12259. (i) Gersten, S. W.; Samuels, G. J.; Meyer, T. J. *J. Am. Chem. Soc.* **1982**, *104*, 4029–4030.

(3) (a) Humphreys, K. J.; Mirica, L. M.; Wang, Y.; Klinman, J. P. *J. Am. Chem. Soc.* **2009**, *131*, 4657–4663. (b) Roth, J. P. *Acc. Chem. Res.* **2009**, *42*, 399–408. (c) Meyer, T. J.; Huynh, M. H. V.; Thorp, H. H. *Angew. Chem., Int. Ed.* **2007**, *46*, 5284–5304. (d) Roth, J. P.; Klinman, J. P. *Proc. Natl. Acad. Sci. U.S.A.* **2003**, *100*, 62–67. (e) Roth, J. P.; Wincek, R.; Nodet, G.; Edmondson, D. E.; McIntire, W. S.; Klinman, J. P. *J. Am. Chem. Soc.* **2004**, *126*, 15120–15131. (f) Tommos, C.; Babcock, G. T. *Acc. Chem. Res.* **1998**, *31*, 18–25.

(4) (a) Kreutz, J. E.; Shukhaev, A.; Du, W.; Druskin, S.; Daugulis, O.; Ismagilov, R. F. *J. Am. Chem. Soc.* **1010**, *132*, 3128–3132. (b) Zhang, C.; Jiao, N. *J. Am. Chem. Soc.* **2010**, *132*, 28–29. (c) Jia, C.-J.; Liu, Y.; Bongard, H.; Schueth, F. *J. Am. Chem. Soc.* **1010**, *132*, 1520–1522. (d) King, A. E.; Brunold, T. C.; Stahl, S. S. *J. Am. Chem. Soc.* **2009**, *131*, 5044–5045. (e) Hong, S.; Lee, Y.-M.; Shin, W.; Fukuzumi, S.; Nam, W. *J. Am. Chem. Soc.* **2009**, *131*, 13910–13911. (f) Taylor, R. A.; Law, D. J.; Sunley, G. J.; White, A. J. P.; Britovsek, G. J. P. *Angew. Chem., Int. Ed.* **2009**, *48*, 5900–5903. (g) Matienko, L. I.; Mosolova, L. A.; Zaikov, G. E. *Russ. Chem. Rev.* **2009**, *78*, 211–230. (h) Berkessel, A. Special issue on the activation of dioxygen and homogeneous catalytic oxidation. *J. Mol. Catal. A* **2006**, *251*, 1−298. (i) Cornell, C. N.; Sigman, M. S. In *Activation of Small Molecules*; Tolman, W. B., Ed.; Wiley-VCH: Weinheim, 2006; pp 159−186.

(5) (a) Nocera, D. G., Guldi, D. Guest Eds. Special issue on renewable energy. *Chem. Soc. Rev.* **2009**, *38*, 1−300. (b) Eisenberg, R., Nocera, D. G., Guest Eds. Forum on solar and renewable energy. *Inorg. Chem.* **2005**, *44*, 6799−7260.

(6) (a) Weinstock, I. A. *Inorg. Chem.* **2008**, *47*, 404–406. (b) Geletii, Y. V.; Hill, C. L.; Atalla, R. H.; Weinstock, I. A. *J. Am. Chem. Soc.* **2006**, *128*, 17033–17042. (c) Geletii, Y. V.; Hill, C. L.; Bailey, A. J.; Hardcastle, K. I.; Atalla, R. H.; Weinstock, I. A. *Inorg. Chem.* **2005**, *44*, 8955–8966.

(7) (a) Weinstock, I. A.; Barbuzzi, E. M. G.; Wemple, M. W.; Cowan, J. J.; Reiner, R. S.; Sonnen, D. M.; Heintz, R. A.; Bond, J. S.; Hill, C. L. *Nature* **2001**, *414*, 191–195. (b) Cowan, J. J.; Bailey, A. J.; Heintz, R. A.; Do, B. T.; Hardcastle, K. I.; Hill, C. L.; Weinstock, I. A. *Inorg. Chem.* **2001**, *40*, 6666–6675. (c) Weinstock, I. A.; Cowan, J. J.; Barbuzzi, E. M. G.; Zeng, H.; Hill, C. L. *J. Am. Chem. Soc.* **1999**, *121*, 4608–4617.

(8) Sawyer, D. T.; Valentine, J. S. *Acc. Chem. Res.* **1981**, *14*, 393–400.

(9) For recent review articles on this topic, see: (a) Costentin, C. *Chem. Rev.* **2008**, *108*, 2145–2179. (b) Hammes-Schiffer, S.; Hatcher, E.; Ishikita, I.; Skone, J. H.; Soudackov, A. V. *Coord. Chem. Rev.* **2008**, *252*, 384–394. (c) Huynh, M. H. V.; Meyer, T. J. *Chem. Rev.* **2007**, *107*, 5004–5064. (d) Mayer, J. M. *Annu. Rev. Phys. Chem.* **2004**, *55*, 363–90.

(10) The abbreviation CPET follows Mayer and Savéant[10a,d] and is synonymous with CEP used by Nocera and Hammarström.[10c] Meyer[9c] refers to this more precisely as "multi-site electron−proton transfer" (MS-EPT). (a) Markle, T. F.; Rhile, I. J.; DiPasquale, A. G.; Mayer, M. J. *Proc. Natl. Acad. Sci. U.S.A.* **2008**, *105*, 8185–8190. (b) Hammes-Schiffer, S.; Soudackov, A. V. *J. Phys. Chem. B* **2008**, *112*, 14108–14123. (c) Irebo, T.; Reece, S. Y.; Sjodin, M.; Nocera, D. G.; Hammarström, L. *J. Am. Chem. Soc.* **2007**, *129*, 15462–15464. (d) Costentin, C.; Robert, M.; Savéant, J.-M. *J. Am. Chem. Soc.* **2007**, *129*, 5870–5879.

(11) For important specific examples of concerted multisite electron−proton transfer *to multisite acceptors*, see refs 3c and 12.

(12) (a) Roth, J. P.; Lovell, S.; Mayer, J. M. *J. Am. Chem. Soc.* **2000**, *122*, 5486–5498. (b) Hoganson, C. W.; Babcock, G. T. *Science* **1997**, *277*, 1953–1956. (c) Fenwick, C. W.; English, A. M.; Wishart, J. F. *J. Am. Chem. Soc.* **1997**, *119*, 4758–4764. (d) Binstead, R. A.; Meyer, T. J. *J. Am. Chem. Soc.* **1987**, *109*, 3287–3297.

(13) Costentin, C.; Robert, M.; Savéant, J. M. *J. Phys. Chem. C* **2007**, *111*, 12877–12880.

(14) Chanon, M.; Julliard, M.; Santamaria, J.; Chanon, F. *New J. Chem.* **1992**, *16*, 171–201.

(15) (a) Irebo, T.; Johansson, O.; Hammarström, L. *J. Am. Chem. Soc.* **2008**, *130*, 9194–9195. (b) Fecenko, C. J.; Meyer, T. J.; Thorp, H. H. *J. Am. Chem. Soc.* **2006**, *128*, 11020–11021. (c) Sjodin, M.; Styring, S.; Wolpher, H.; Xu, Y.; Sun, L.; Hammarström, L. *J. Am. Chem. Soc.* **2005**, *127*, 3855–3863. (d) Reece, S. Y.; Nocera, D. G. *J. Am. Chem. Soc.* **2005**, *127*, 9448–9458. (e) Sjodin, M.; Styring, S.; Akermark, B.; Sun, L.; Hammarström, L. *J. Am. Chem. Soc.* **2000**, *122*, 3932–3936.

(16) (a) Markle, T. F.; Mayer, J. M. *Angew. Chem., Int. Ed.* **2008**, *47*, 738–740. (b) Costentin, C.; Robert, M.; Savéant, J. M. *J. Am. Chem. Soc.* **2007**, *129*, 9953–9963. (c) Costentin, C.; Robert, M.; Savéant, J. M. *J. Am. Chem. Soc.* **2006**, *128*, 4552–4553. (d) Rhile, I. J.; Markle, T. F.; Nagao, H.; DiPasquale, A. G.; Lam, O. P.; Lockwood, M. A.; Rotter, K.; Mayer, J. M. *J. Am. Chem. Soc.* **2006**, 6075–6088. (e) Cape, J. L.; Bowman, M. K.; Kramer, D. M. *J. Am. Chem. Soc.* **2005**, *127*, 4208–4215. (f) Rhile, I. J.; Mayer, J. M. *J. Am. Chem. Soc.* **2004**, *126*, 12718–12719. (g) Cukier, R. I.; Nocera, D. G. *Annu. Rev. Phys. Chem.* **1998**, *49*, 337–369.

(17) Ishikita, H.; Soudackov, A. V.; Hammes-Schiffer, S. *J. Am. Chem. Soc.* **2007**, *129*, 11146–11152.

Hence, discovery of the multisite CPET in Figure 1 not only is an important advance in understanding the reactivity of dioxygen in water, and relevant to numerous O_2-based processes, but also introduces a fundamentally new type of CPET reaction. Its novel mechanism emerges from detailed analysis of the microscopic steps responsible for the simultaneous coupling of reactions between $\mathbf{1}_{1e}$, O_2, and H^+. As will be shown, this formally termolecular process is facilitated by the unique behavior of hydrated protons in water.[19]

Materials and Methods

Synthesis and Characterization. Fully oxidized α-Keggin ions and one Wells−Dawson ion [POM_{ox}; all W atoms in their highest, 6+, d^0, oxidation states: α-$H_3P^{V}W_{12}O_{40}$ ($H_3\mathbf{1}_{ox}$),[20] α-$H_4Si^{IV}W_{12}O_{40}$ ($H_4\mathbf{2}_{ox}$),[20] α-$H_5Al^{III}W_{12}O_{40}$ ($H_5\mathbf{3}_{ox}$),[21] and α-$K_6P_2W_{18}O_{68}$ ($K_6\mathbf{4}_{ox}$)[22]] were prepared by published methods. One-electron-reduced forms of the above anions [POM_{1e}; α-$P^{V}W_{12}O_{40}^{4-}$ ($\mathbf{1}_{1e}$), α-$Si^{IV}W_{12}O_{40}^{5-}$ ($\mathbf{2}_{1e}$), α-$Al^{III}W_{12}O_{40}^{6-}$ ($\mathbf{3}_{1e}$), and α-$P_2W_{18}O_{68}^{7-}$ ($\mathbf{4}_{1e}$)] were prepared in water at appropriate pH values by constant-potential electrolysis, as previously described[6b,c] for **1** and **3**, and stored under argon. At pH 2.1 in $NaHSO_4$ buffer, extinction coefficients are $\epsilon_{750} = (1.82 \pm 0.1) \times 10^3\ M^{-1}\ cm^{-1}$ for $\mathbf{1}_{1e}$ and, from previous work,[6b,c] $\epsilon_{700} = (1.48 \pm 0.1) \times 10^3\ M^{-1}\ cm^{-1}$ for $\mathbf{2}_{1e}$ and $(1.8 \pm 0.1) \times 10^3\ M^{-1}\ cm^{-1}$ for $\mathbf{3}_{1e}$. For kinetic work, high-purity aq HCl was prepared by gas transfer (as described below); all other materials were obtained from commercial sources.

Aqueous Solutions. Solutions were prepared using 18.2 MΩ water from a Millipore (Direct-Q 5 Ultrapure) water purification system, and added salts were of the highest purity available. Highly pure HCl solutions were prepared by distillation from reagent-grade concentrated 10.2 M HCl (Gadot Lab Supplies, Israel). For this, the concentrated HCl was placed in a round-bottom flask with a side arm, covered with a rubber septum, and heated in an oil bath to between 60 and 70 °C. An inert carrier gas (argon or nitrogen) was bubbled through the HCl solution via the septum, using a needle fitted with Teflon tubing whose tip was submerged under the surface of the solution. The HCl-enriched atmosphere above the solution was directed through commercial silicon hosing into pure water in an ice-bath-cooled narrow-mouth bottle. Final $[H^+]$ values were determined by acid−base titration using phenolphthalein. Obtained solutions were between 2.6 and 8.4 M in HCl and were stored at 5 °C in collection bottles fitted with Teflon-lined plastic caps. In most kinetic work, ionic strength was kept constant at 2.0 M by addition of LiCl.

Instrumentation. UV−vis spectra and reaction rate data were obtained using a Hewlett-Packard 8452A spectrophotometer equipped with a diode-array detector, and a Julabo F-12 (±0.1 °C) temperature controller was used to maintain specified temperatures in the sample cell of the spectrophotometer to within ±1 °C for work done near room temperature. When needed for characterization of literature compounds, ^{31}P, ^{29}Si, and ^{27}Al NMR spectra of polyoxometalate (POM) salts in D_2O or water/D_2O mixtures were acquired using a Brüker 500 MHz instrument, using previously reported parameters (a more critical issue for acquisition of the less routine ^{27}Al spectra).[7,23] Fourier transform infrared (FTIR) spectra were acquired using a Nicolet Impact 410 spectrophotometer (KBr pellets). Electrochemical data were obtained at room temperature using a CHI 760 electrochemical station equipped with a glassy-carbon working electrode, a Pt-wire auxiliary electrode, and a Ag/AgCl (3 M NaCl) reference electrode. Bulk electrolyses were done using a BAS reticulated glassy carbon working electrode and a Pt coil auxiliary electrode separated from the solution by a suitable compartment equipped with a glass frit. Reduction potentials are reported relative to the normal hydrogen electrode (NHE). pH measurements were made using an Eutech Instruments pH510 pH meter.

Electrochemistry. Cyclic voltammetry (CV) data[6b,c] were obtained at ambient temperature (22 ± 2 °C) using 1.5−5 mM POM salts in aq HCl (if constant ionc strength was maintained, LiCl was added). Unless specified, scan rates were 100 mV s^{-1}. The Ag/AgCl (3 M NaCl) reference electrode was calibrated in previous work,[6c] and reported $E_{1/2}$ values were referenced to the NHE by addition of 250 mV.[6c] Solutions of $1e^-$-reduced α-Keggin anions were prepared by bulk electrolysis[6b,c] under Ar.

O_2 Concentrations. The concentration of O_2 in pure water at 25 °C and 1 atm O_2 is 1.24 mM. The solubility of O_2 is smaller in aqueous electrolyte solutions than in pure water and depends strongly on salt concentration and, to a lesser extent, on the nature of the electrolyte. In this work, total salt concentrations were typically high (ca. between 0.1 and 2.0 M) and therefore decreased saturated O_2 concentrations. Because the solutions contained mixed electrolytes, published $[O_2]$ values for the actual salt compositions of the solutions were not available. Instead, tabulated data and empirically determined solubility functions[24] were used to calculate specific $[O_2]$ values for each of the solutions studied. Estimated solubilities ranged from 0.97 to 1.13 mM O_2. Temperature dependence experiments were conducted over a range from 5 to 45 °C, and the effect of temperature on O_2 solubility at each of the salt concentrations used was accounted for in a similar fashion. In these experiments, $[O_2]$ values ranged from 0.80 to 1.27 mM. When these $[O_2]$ values were used to obtain rate constants, error analysis showed that reasonable uncertainties in calculated O_2 solubilities were much smaller than the effects of $[H^+]$ on rates. This is particularly true for reactions at constant ionic strength, where the variations in $[O_2]$ due to replacement of Li^+ by H^+ are small. In most kinetic runs, aliquots of O_2-free POM_{1e} solutions were added in 1:9 v:v ratios to thermally equilibrated electrolyte solutions saturated with O_2 or air.

Reaction Stoichiometry. Previous work[6b] demonstrated that 2 equiv of reduced POM anions ($POM_{1e} = \mathbf{1}_{1e}$, $\mathbf{2}_{1e}$, or $\mathbf{3}_{1e}$) react with O_2 to give H_2O_2 (eq 2), while other published data show that reductions of H_2O_2 by heteropolytungstates are at least an order of magnitude slower than reactions of the same heteropolytungstates with O_2.[25]

$$2POM_{1e} + 2H^+ + O_2 \rightarrow 2POM_{ox} + H_2O_2 \qquad (2)$$

In previous work,[6b] reactions of $\mathbf{3}_{1e}$ with O_2 were studied at pH values between 1.8 and 7, while reactions of $\mathbf{1}_{1e}$ were studied only at the lower pH value of 1.8 (hydrolytic decomposition occurs at higher pH values). In the present study, rates of oxidation of $\mathbf{1}_{1e}$ by O_2 are studied at $[H^+]$ values between 0.1 and 1.9 M. Rates

(18) (a) Song, N.; Stanbury, D. M. *Inorg. Chem.* **2008**, *47*, 11458–11460. (b) Sjödin, M.; Ghanem, R.; Polivka, T.; Pan, J.; Styring, S.; Sun, L.; Sundström, V.; Hammarström, L. *Phys. Chem. Chem. Phys.* **2004**, *6*, 4851–4858. (c) Carra, C.; Iordanova, N.; Hammes-Schiffer, S. *J. Am. Chem. Soc.* **2003**, *125*, 10429–10436.

(19) (a) Marx, D.; Chandra, A.; Tuckerman, M. E. *Chem. Rev.* **2010**, *110*, 2174–2216. (b) Stoyanov, E. S.; Stoyanova, I. V.; Reed, C. A. *J. Am. Chem. Soc.* **2010**, *132*, 1484–1485. (c) Swanson, J. M. J.; Simons, J. *J. Phys. Chem. B* **2009**, *113*, 5149–5161. (d) Siwick, B. J.; Cox, M. J.; Bakker, H. J. *J. Phys. Chem. B* **2008**, *112*, 378–389. (e) Marx, D. *ChemPhysChem* **2006**, *7*, 1848–1870. (f) Mohammed, O. F.; Pines, D.; Dreyer, J.; Pines, E.; Nibbering, E. T. J. *Science* **2005**, *310*, 83–86. (g) Hynes, J. T. *Nature* **1999**, *397*, 565–566. (h) Marx, D.; Tuckerman, M. E.; Hutter, J.; Parrinello, M. *Nature* **1999**, *397*, 601–604. (i) Agmon, N. *Chem. Phys. Lett.* **1995**, *244*, 456–462. (j) Eigen, M. *Angew. Chem., Int. Ed.* **1964**, *3*, 1–19.

(20) Pope, M. T.; Varga, G. M., Jr. *Inorg. Chem.* **1966**, *5*, 1249–1254.

(21) Cowan, J. J.; Hill, C. L.; Reiner, R. S.; Weinstock, I. A. *Inorg. Synth.* **2002**, *33*, 18–26.

(22) Graham, C. R.; Finke, R. G. *Inorg. Chem.* **2008**, *47*, 3679–3686.

(23) Akitt, J. W. Structural Determination of Inorganic Compounds. In *Modern NMR Techniques and Their Applications in Chemistry*; Popov, A. I., Hallenga, K., Eds.; M. Dekker: New York, 1991; Vol. 11.

(24) Clever, H. L.; Young, C. L.; Battino, R.; Derrick, M. E.; Katovic, V.; Pogrebnaya, V. L.; Usov, A. P.; Baranov, A. V. *Solubility Data Series* **1981**, *7*, 56–189.

(25) Weinstock, I. A. *Chem. Rev.* **1998**, *98*, 113–170.

observed at 0.1 M H^+ are in line with those reported previously at pH 1.8 (0.016 M H^+), aside from small differences due to changes in electrolytes and ionic strengths.

Two sets of control experiments were carried out to ensure that variations in rate constants observed at large $[H^+]$ values (0.1−1.9 M) were not due to more rapid, H^+-dependent reactions of $\mathbf{1}_{1e}$ with product H_2O_2. In the first set, solutions of $\mathbf{1}_{1e}$ were rapidly mixed with solutions uniformly saturated with O_2 but that also contained *deliberately added* H_2O_2. Rates of consumption of $\mathbf{1}_{1e}$ at $[H^+]$ = 0.1 and 1.9 M were quantified by UV−visible spectroscopy at two H_2O_2 concentrations: 0.128 and 0.256 mM. These concentrations correspond (respectively) to 70 and 150% of the total concentration of H_2O_2 expected on the basis of the stoichiometry of the reaction in eq 2. *Observed rate constants were statistically indistinguishable from those obtained in the absence of initially added peroxide*, i.e., less than the 2−3% uncertainties in calculated k_{app} values (Figure S1 and Table S1, Supporting Information).

In the second set of experiments, $\mathbf{1}_{1e}$ was completely oxidized by O_2 (1 atm) at 0.1 and 1.9 M H^+ (in the absence of LiCl), and concentrations of H_2O_2 produced were quantified by reaction with I^-.[26] A fresh solution containing 0.16 M KI, 6.4×10^{-5} M ammonium heptamolybdate, and 0.002 M KOH was prepared and immediately mixed in a 1:1 v:v ratio with a solution of 0.04 M potassium hydrogen phthalate to give a final pH of ∼4. Although the oxidation of I^- by atmospheric O_2 is relatively slow at pH 4, the solutions were used immediately. After complete reaction of $\mathbf{1}_{1e}$ with O_2 (indicated by discharge of the blue color), an aliquot was added to the I^- solution. Aliquot volumes were adjusted to keep final H_2O_2 concentrations between 1 and 10 μM, and H_2O_2 was quantified by measuring the absorbance of I_3^- at 350 nm (ε_{350} = 26 500 M^{-1} cm^{-1}). After completion of reaction at both 0.1 and 1.9 M H^+, 0.50 ± 0.01 equiv of H_2O_2 was produced per equivalent of $\mathbf{1}_{1e}$, precisely as indicated in eq 2.

These control experiments unequivocally demonstrate that, at all $[H^+]$ values used in this work, 2 equivs of $\mathbf{1}_{1e}$ are consumed by each equivalent of O_2 and that the oxidation of $\mathbf{1}_{1e}$ by H_2O_2 (product) is not kinetically significant.

Kinetic Measurements. Reactions of $\mathbf{1}_{1e}$ were carried out in water and in D_2O at H^+ (D^+) concentrations from 0.1 to 1.9 M. Unless indicated, ionic strength, μ, was kept constant at 2.00 ± 0.02 M. The uncertainty is due to contributions from [POM] values, which were always small (several mM) but not strictly constant. In most kinetic runs, >90% of each reaction was recorded, and ionic strength values changed as the POMs were oxidized by O_2. In a number of cases, reactions were carried out without the addition of LiCl, and the ionic strength varied with $[H^+]$. Reactions of $\mathbf{1}_{1e}$ with O_2 were carried out in a series of nine solutions, from 0.10 to 1.90 M H^+, with LiCl added to maintain the ionic strength. For reactions of $\mathbf{2}_{1e}$, $\mathbf{3}_{1e}$, and $\mathbf{4}_{1e}$, five $[H^+]$ values between 0.10 and 1.90 M H^+ were used. For $\mathbf{4}_{1e}$, the K^+ (countercation) concentrations were several orders of magnitude smaller than added $[H^+]$ and/or $[Li^+]$; for the other POMs, H^+ countercation concentrations were explicitly included.

The general method is described for reactions of $\mathbf{1}_{1e}$: A cuvette filled with 2.25 mL of an electrolyte solution containing HCl (with or without LiCl) was placed in the observation compartment of the UV−vis spectrometer, previously set at 25 ± 0.1 °C. A 1-mm-o.d. Teflon tube was used to bubble hydrated pure O_2 into the solution in the cuvette for 10 min. The tube was directed to a sidewall of the cuvette so that the bubbles did not interrupt the instrument's optical path. Next, 0.25 mL of an O_2-free solution of $\mathbf{1}_{1e}$ was added to the cuvette, and absorbance versus time data were recorded at 750 nm. Initial mixing was achieved using the bubble stream, which also kept the solution saturated with O_2 (i.e., at a constant $[O_2]$). The observation wavelength was chosen after inspecting the UV−vis spectra of the $1e^-$-reduced and fully oxidized α-Keggin anions. Typically, 90% completion of each reaction was used to obtain pseudo-first-order rate constants (i.e., for changes in $[\mathbf{1}_{1e}]$ at constant $[O_2]$).

Because $\mathbf{4}_{1e}$ reacts very slowly with O_2, the reactions were followed at 25 °C for the first 2% change in the POM absorbance (5−10 min), and rate constants were calculated using an initial-rate method. This approach minimized the evaporative loss of HCl caused by bubbling of O_2 through the solution.

For variable-temperature experiments using $\mathbf{1}_{1e}$ at elevated temperatures, initial rates were measured (10% of each reaction) using ambient air as the source of O_2. Dioxygen concentrations were calculated from tabulated data as functions of both electrolyte and temperature.[24]

Uncertainties associated with experimental rate constants—standard deviations from multiple runs (typically 3−9 runs for each k value)—varied from <1.7 to 9%. An additional ±2% error was introduced through calculations of $[O_2]$ values from tabular data and possible small changes in $[H^+]$ due to bubbling of O_2 into aq HCl solutions prior to POM_{1e} addition. The average uncertainty was ±6%.

Rate Constants. Rate constants were obtained by nonlinear exponential fittings (OriginLab 8.0) to the expression in eq 3, with k_{app} and A_∞ as variable parameters.

$$A = A_0 \exp(-k_{app}t) + A_\infty \tag{3}$$

Correlation coefficients, R^2, obtained using this method were generally >0.999. For temperature-dependence experiments and for reactions of $\mathbf{4}_{1e}$, reactions were followed to 10% and to 2%, respectively. In these cases, Microsoft Excel was used to calculate k_{app} as $[\Delta A/\Delta(t)]/A_0$, where ΔA is initial absorbance minus absorbance at time t, Δt is final t minus initial t, and A_0 is initial absorbance, and the slopes of these lines were taken as values for the apparent rate constant, k_{app}. Reactions at each set of conditions were typically carried out four or five times, and these repetitions also confirmed that variations in A_0 had no effect on k_{app} values. The k_{app} values were divided by $[O_2]$ to give the rate constants, k_{obs}, defined in eq 4.

$$-\mathrm{d}[\mathbf{1}_{1e}]/\mathrm{d}t = k_{obs}[\mathbf{1}_{1e}][O_2] \tag{4}$$

As previously reported,[6b] 2 equivs of $\mathbf{1}_{1e}$ are consumed by each equivalent of O_2 (to give the initial product, H_2O_2), such that the rate constant, k, for the rate-limiting transfer of the first electron to O_2 is described by eq 5.

$$-\mathrm{d}[\mathbf{1}_{1e}]/\mathrm{d}t = k_{obs}[\mathbf{1}_{1e}][O_2] = 2k[\mathbf{1}_{1e}][O_2] \tag{5}$$

More detailed evaluation of k as a function of $[H^+]$—the subject of this report—is provided in the Results and Discussion sections. To ensure accuracy and reproducibility, all rate constants (pseudo-first-order or initial-rate methods) were measured between 3 and 10 times.

Anearobic Reactions (To Exclude Reduction of H^+ by $\mathbf{1}_{1e}$). In order to verify that the reduction of dioxygen by $\mathbf{1}_{1e}$ at large $[H^+]$ occurs by ET from the POM to O_2, rather than via the reduction of H^+ to H-atom intermediates, $\mathbf{1}_{1e}$ was reacted with HCl in the absence of O_2. A 2.0 M HCl solution was prepared, moved to a cuvette, and degassed by bubbling with gaseous Ar. Next, 0.25 mL of 5 mM $\mathbf{1}_{1e}$ was added with continuous bubbling of Ar. After 13 min, the absorbance at 750 nm remained effectively constant; i.e., $\mathbf{1}_{1e}$ was not oxidized by H^+. (A negligible decrease of 0.03 au, ∼5% relative to a typical reaction with 1 mM O_2, was observed, probably due to the presence of trace amounts of O_2.)

Effect of Added $\mathbf{1}_{ox}$. The oxidized form of **1** (i.e., $\mathbf{1}_{ox}$) was used to determine whether the first one-electron step is reversible. This was done by starting with a reacting system containing 0.3 mM $\mathbf{1}_{1e}$ and 0.2 mM $\mathbf{1}_{ox}$, prepared by partial oxidation of a solution

(26) (a) Meyerstein, D.; Treinin, A. *Trans. Faraday Soc* **1963**, *59*, 1114–1120. (b) Rachmilovich-Calis, S.; Masarwa, A.; Meyerstein, N.; Meyerstein, D.; van Eldik, R. *Chem.—Eur. J.* **2009**, *15*, 8303–8309.

originally 0.5 mM in $\mathbf{1}_{1e}$ at 0.1 M HCl (1.6 M LiCl). This solution was then made 0.5 mM in $\mathbf{1}_{ox}$, and the reaction continued. Apparent rate constants were the same as those obtained without added $\mathbf{1}_{ox}$.

Kinetic Isotope Effects. Rate constants were determined in two ways: (1) using 1.9 M $H^+(D^+)$ at constant ionic strength and incrementally increasing D_2O:H_2O v:v ratios, and (2) as a function of $[D^+]$ in 75% D_2O with no added electrolyte (variable ionic strength). First, a solution of DCl free of trace metal impurities was prepared by transferring HCl(g) to a collecting vessel that contained pure D_2O. The method used was analogous to that described above for the preparation of "aqueous solutions". The final 2.0−6.4 M acid solutions contained predominantly DCl in D_2O, with small (≤ca. 5%) concentrations of HDO and HCl. $[D^+]$ values were determined by acid−base titration, and experimental uncertainties due to HDO and HCl were minimized by subsequent dilutions with D_2O. Solutions of 1.9 M acid were then prepared at $[H^+]/[D^+]$ ratios of 0, 22.5, 45, and 67.5% by combining 1.9 M HCl in H_2O with 1.9 M DCl in D_2O at corresponding v:v ratios. Kinetic isotope effect data for reactions of $\mathbf{1}_{1e}$ were obtained at 25 ± 1 °C. The effect of increases in $[D^+]$ was determined by adding HCl to 75% D_2O solutions such that $0.75D^+ + 0.25H^+$ equaled 0.10, 0.66, 1.22, and 1.82 M. For both methods, k_{app} values were determined using O_2-saturated solutions (constant 1 atm O_2), using the pseudo-first-order analysis described above.

Note on Catalysis by Trace Quantities of Cu. Cu ions are known to catalyze ET to O_2 (see ref 6b and articles cited therein). When [Cu] was not carefully excluded, irregularities in kinetic data were observed. At the large $[H^+]$ values used in this work, chelating agents such as diethylenetriaminepentaacetic acid (DTPA) and neocuproine are not effective. Therefore, to avoid Cu catalysis, extra care was taken, and in some cases the entire procedure—from POM synthesis through the acquisition of kinetic data—had to be repeated. Specifically, high-purity HCl was prepared by distillation as described above. In addition, DTPA (2 mM at pH 5−6) was used to rinse all glassware and apparatus that came in contact with the reactant solutions. In some cases, the Keggin ion salts themselves were prepared with extra care taken to avoid traces of copper in reagents used, and with prior washing of all equipment with DTPA solutions. Finally, to control for possible Cu contamination from LiCl, high-purity LiCl was used, and control experiments were carried out with no added LiCl. *These extra steps made it possible to observe well-behaved kinetics and rate constants uncompromised by Cu catalysis at all $[H^+]$ studied.* In the absence of kinetically significant Cu catalysis, correlation coefficients R^2 were typically >0.9999%, while for Cu-compromised reactions, values of R^2 < 0.99% and poor reproducibility were observed. Hence, in cases where Cu catalysis was not successfully minimized, the consequences were readily apparent, and necessary steps were taken, even if this meant starting again with new POM syntheses.

Results

Previous work established that ET from one-electron-reduced Keggin heteropolytungstates to O_2 in water occurs via outer-sphere ET.[6a,b] That was accomplished using an isostructural series of $1e^-$-reduced anions, α-Keggin-$X^{n+}W_{12}O_{40}^{(9-n)-}$, whose charges increased from 4− to 5− to 6− as the central heteroatom, X^{n+}, varied from P^{5+} to Si^{4+} to Al^{3+} ($\mathbf{1}_{1e}$, $\mathbf{2}_{1e}$, and $\mathbf{3}_{1e}$, respectively). The three cluster anions were studied using pH ranges at which each is stable to hydrolysis. Hence, $\mathbf{1}_{1e}$ and $\mathbf{2}_{1e}$ were studied at pH 1.8 (sulfate buffer), while $\mathbf{3}_{1e}$, which is considerably more stable to hydrolysis, was studied at pH values from 1.8 to 7.[6a,b] In all these cases, rate-limiting ET to O_2 occurs via an outer-sphere mechanism. The pK_a of $HO_2^{\bullet}$ is 4.7, such that, at pH 1.8, ET to O_2 is followed by rapid PT to $O_2^{\bullet-}$ (an ETPT mechanism).

We now address ET to O_2 at larger H^+ concentrations. As before,[6] due attention is paid to possible association between

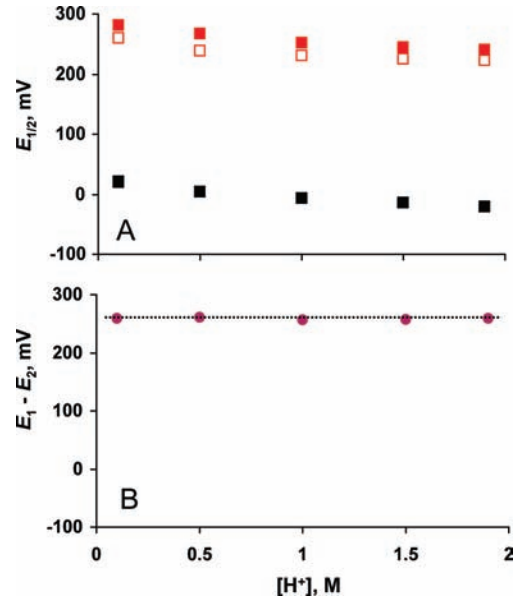

Figure 2. First and second one-electron reduction potentials of α-$PW_{12}O_{40}^{3-}$ ($\mathbf{1}_{ox}$) as a function of $[H^+]$ at 2.0 M ionic strength, maintained by addition of LiCl. (A) First (solid red squares) and second (solid black squares) one-electron reduction potentials. The open red squares are the first one-electron reduction potentials in the absence of LiCl. (B) Solid circles indicate the difference (in mV) between the first and second one-electron reduction potentials in panel A (constant ionic strength). All couples were electrochemically reversible, with the exception of 0.1 M H^+ (no added LiCl) for which, due to the small electrolyte concentration, quasi-reversible behavior was observed.

H^+ or electrolyte cations and the oxidized and reduced forms of the POM anions. This is important because protonation[27] (and ion-pairing generally)[28] shifts the reduction potentials of POM_{ox}/POM_{1e} couples to more positive values, thereby effecting Gibbs free energies, mechanisms,[29] and rates of ET.[25] Of the three anions studied, α-$PW_{12}O_{40}^{3-}$ ($\mathbf{1}_{ox}$) has the smallest negative charge and is least subject to alkali-metal cation or proton association in solution. Its reactions with O_2 are also the most endergonic.[6a,b,20] The effects of $[H^+]$ on ET from $\mathbf{1}_{1e}$ to O_2 are now described in detail, along with control and other experiments that document the emergence of a multisite CPET pathway at $[H^+]$ values larger than 0.3 M.

Solution-State Characterization. The solution-state properties of $\mathbf{1}_{ox}$ and $\mathbf{1}_{1e}$ were evaluated by CV to confirm that no significant ion-pairing occurs as $[H^+]$ values are varied from 0.1 to 1.9 M at constant ionic strength. LiCl was chosen to maintain constant ionic strength because, of all alkali-metal cations, Li^+ has the least tendency to associate with Keggin anions in water.[30]

The first and second one-electron reduction potentials of $\mathbf{1}_{ox}$ (the α-$PW_{12}O_{40}^{3-}$/α-$PW_{12}O_{40}^{4-}$ and α-$PW_{12}O_{40}^{4-}$/α-$PW_{12}O_{40}^{5-}$ couples, respectively) were determined at $[H^+]$ values from 0.1 to 1.9 M at constant ionic strength (Figure 2A). These data provide two diagnostic indications that neither $\mathbf{1}_{ox}$ nor $\mathbf{1}_{1e}$ is

(27) Guo, S.-G.; Mariotti, A. W. A.; Schlipf, C.; Bond, A. M.; Wedd, A. G. *Inorg. Chem.* **2006**, *45*, 8563–8574.
(28) Antonio, M. R.; Nyman, M.; Anderson, T. A. *Angew. Chem., Int. Ed.* **2009**, *48*, 6136–6140.
(29) (a) Czap, A.; Neuman, N. I.; Swaddle, T. W. *Inorg. Chem.* **2006**, *45*, 9518–9530. (b) Grigoriev, V. A.; Cheng, D.; Hill, C. L.; Weinstock, I. A. *J. Am. Chem. Soc.* **2001**, *123*, 5292–5307. (c) Prenzler, P. D.; Boskovic, C.; Bond, A. M.; Wedd, A. G. *Anal. Chem.* **1999**, *71*, 3650–3656.
(30) Kirby, J. F.; Baker, L. C. W. *Inorg. Chem.* **1998**, *37*, 5537–5543.

significantly protonated or associated with Li^+ over the pH range studied.[31] First, very similar one-electron reduction potentials are observed when no LiCl is added (open red squares in Figure 2A). Second, the *difference* between the first and second reduction potentials remains effectively constant, within ±2 mV, as Li^+ is replaced by H^+ at constant ionic strength (Figure 2B). These data demonstrate that, at 2 M ionic strength, ion-pairing with either Li^+ or H^+ is not significant for α-$PW_{12}O_{40}^{4-}$ ($\mathbf{1}_{1e}$) or for the more highly charged two-electron-reduced anion, α-$PW_{12}O_{40}^{5-}$.

Reaction Stoichiometry at Large H^+ Concentrations. Having confirmed that both $\mathbf{1}_{ox}$ and $\mathbf{1}_{1e}$ are effectively free of H^+ and Li^+ association at constant (2 M) ionic strength, we next obtained absorbance versus time data at 750 nm for the reaction between $\mathbf{1}_{1e}$ and O_2 at H^+ concentrations from 0.1 to 1.9 M (Figure S2, Supporting Information). Solutions were saturated with a hydrated stream of pure O_2 (1 atm), which was bubbled through the solution before and during data acquisition. Apparent rate constants, k_{app}, were obtained from pseudo-first-order fits to exponential decreases in absorbance at constant $[O_2]$. Observed rate constants, k_{obs}, were obtained by dividing k_{app} values by $[O_2]$ calculated using published data[24] (see Materials and Methods).

At 0.1 M H^+, the observed rate constant, k_{obs}, was 2.4 M^{-1} s^{-1}, close to the value of 2.8 M^{-1} s^{-1} reported previously[6b] for reaction at pH 1.8 (0.016 M H^+) in $NaHSO_4$ buffer at 175 mM ionic strength. In both cases, the balanced equation for reduction of O_2 to H_2O_2 is as shown in eq 6.

$$2\mathbf{1}_{1e} + O_2 + 2H^+ \rightarrow 2\mathbf{1}_{ox} + H_2O_2 \qquad (6)$$

To ensure that the stoichiometry in eq 6 remained applicable as $[H^+]$ values were increased from 0.1 to 1.9 M, H_2O_2 was quantified by reaction with I^-. At both 0.1 and 1.9 M H^+, 0.5 equiv of H_2O_2 per equivalent of $\mathbf{1}_{1e}$ was present after complete oxidation of $\mathbf{1}_{1e}$ to $\mathbf{1}_{ox}$ by O_2.

Additional control experiments, described in the Materials and Methods section (see also Figure S1 and Table S1), further demonstrated that product H_2O_2 had no effect on measured rates of O_2 reduction. At the smallest and largest $[H^+]$ values studied (0.1 and 1.9 M), additions of ca. 1 equiv of H_2O_2 to the oxygenated electrolyte solutions prior to additions of $\mathbf{1}_{1e}$ had no significant effect on k_{obs} values.

Other control experiments demonstrated that k_{obs} values were independent of the concentration of the oxidized form of the Keggin ion, $\mathbf{1}_{ox}$, i.e., that the first one-electron step is irreversible. In addition, analysis in previous work[6b] showed that, at pH 1.8, reductions of $HO_2^\bullet$ to H_2O_2 by the one-electron-reduced heteropolytungstate anions, $\mathbf{1}_{1e}$, $\mathbf{2}_{1e}$, and $\mathbf{3}_{1e}$, are faster than superoxide disproportionation. Analogous calculations confirm that the same is true for reactions of $\mathbf{1}_{1e}$ with O_2 at $[H^+]$ values larger than 0.1 M. Accordingly, rate constants, k, for rate-limiting ET to O_2 are obtained by dividing k_{obs} values by 2, i.e., $k = k_{obs}/2$ (see eq 5 in the Materials and Methods section).

(31) The potentials become slightly more negative due to nonlinear change in the activities of the POM anions as the composition of the electrolyte is varied (at constant ionic strength) from 1.9 M LiCl (0.1 M HCl) to 0.1 M LiCl (1.9 M HCl). An analogous change in activities is responsible for the small shift to more negative values at varying ionic strength (no LiCl added; open red squares in Figure 2A). At constant $[Li^+]$, however, H^+ association (protonation) would shift reduction potentials to more *positive* values; this is demonstrated below using $\mathbf{3}_{1e}$.

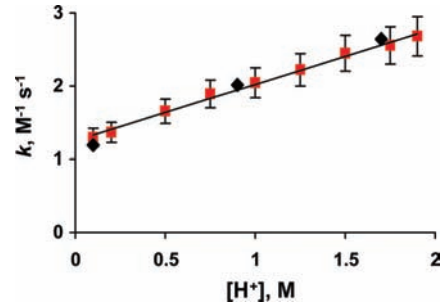

Figure 3. Rate constants, k (= $k_{obs}/2$), for ET to O_2 as a function of $[H^+]$. Red squares are k values as a function of $[H^+]$ at constant ionic strength (2.0 M, by additions of LiCl; $R^2 = 0.994$). Black diamonds at 0.1, 0.9, and 1.7 M H^+ are k values obtained in the absence of added LiCl. The uncertainties associated with the LiCl-free values are similar to those obtained at constant ionic strength.

Scheme 1. ETPT and CPET Pathways

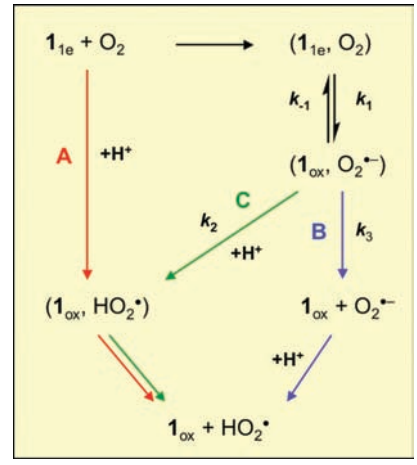

H^+-Dependent Electron Transfer to O_2. As H^+ concentrations increase from 0.1 to 1.9 M, rate constants, k (= $k_{obs}/2$), increase linearly with $[H^+]$ (Figure 3, $R^2 = 0.994$; at 0.3 M H^+, the increase in k is larger than experimental uncertainty). Error analysis indicates that this increase is not an artifact of small changes in $[O_2]$, which varied only slightly with electrolyte composition (but were nevertheless calculated from tabulated values). In addition, statistically identical k values were obtained when $[H^+]$ was varied from 0.1 to 1.7 M *with no added LiCl* (black diamonds). Hence, the increase in k is due neither to changes in association between $\mathbf{1}_{1e}$ and Li^+ nor to variations in "screening factors" associated with electrostatic interactions between reactants and/or products.

As demonstrated immediately below, the linear increase in rate constants, k, in Figure 3 is due to parallel ET (k_{ET}) and CPET ($k_{CPET}[H^+]$) pathways, such that *the first-order dependence on $[H^+]$ results from the involvement of H^+ as a reactant*. This is shown by quantitative analysis of rate expressions for plausible kinetic pathways.

Rate Expressions. Three reaction pathways were considered (Scheme 1; short-lived precursor and successor complexes are shown in parentheses). CPET (path A) is shown in red. A sequential process involving ETPT (path B) is shown in blue. This pathway is independent of $[H^+]$ and was previously established for reductions of O_2 by α-$PW_{12}O_{40}^{4-}$ ($\mathbf{1}_{1e}$), α-$SiW_{12}O_{40}^{5-}$ ($\mathbf{2}_{1e}$), and α-$AlW_{12}O_{40}^{6-}$ ($\mathbf{3}_{1e}$) at pH 1.8.[6b]

Oxidations of the reduced Keggin anions by O_2 are outer-sphere,[6a,b,32] such that there is no bonding interaction between the fully oxidized Keggin ion and $O_2^{\bullet-}$ in the successor−complex ion pairs, e.g., in ($\mathbf{1}_{ox}$,$O_2^{\bullet-}$). Indeed, anion−anion repulsion in these successor complexes is substantial (∼1 kcal mol^{-1} at 0.2 M ionic strength).[6a,b] Moreover, the reorganization energy for back-electron transfer is ca. 25 kcal mol^{-1}. Hence, the anions rapidly separate from one another, as indicted by a diffusion-controlled rate constant, k_3, along path B. At pH values below the pK_a of $HO_2^{\bullet}$ (= 4.7),[8] subsequent steps—protonation of $O_2^{\bullet-}$ and reduction of $HO_2^{\bullet}$ to HO_2^- by a second equivalent of $\mathbf{1}_{1e}$—are both rapid, and no [H$^+$] dependence is observed.[6b]

For completeness, a second ETPT mechanism is now considered (path C, shown in green in Scheme 1). In this hypothetical case, H$^+$ might accelerate the conversion of O_2 to $O_2^{\bullet-}$ by protonating $O_2^{\bullet-}$ ions present at small steady-state concentrations within the successor−complex ion pairs, ($PW_{12}O_{40}^{3-}$,$O_2^{\bullet-}$), abbreviated ($\mathbf{1}_{ox}$,$O_2^{\bullet-}$). For path C to be [H$^+$]-dependent, formation of the successor complexes, ($\mathbf{1}_{ox}$,$O_2^{\bullet-}$), with rate constant k_1, must be reversible, such that back-electron transfer, k_{-1}, competes effectively with k_2, the rate constant for protonation of $O_2^{\bullet-}$ in the short-lived ($\mathbf{1}_{ox}$,$O_2^{\bullet-}$) pairs.

This hypothetical case is analyzed quantitatively using a steady-state approximation in which the concentration of the ($\mathbf{1}_{ox}$,$O_2^{\bullet-}$) pairs remains constant. This gives the rate expression in eq 7 for path C:

$$-\mathrm{d}[\mathbf{1}_{1e}]/\mathrm{d}t = \frac{k_1 k_2[\mathbf{1}_{1e}][O_2][H^+]}{k_{-1} + k_2[H^+]} \qquad (7)$$

The rate constant, k_1, for ET to O_2 is 1.2 M^{-1} s^{-1},[6a,b] and based on electrochemical data—and anion−anion repulsion in the successor complexes, ($\mathbf{1}_{ox}$,$O_2^{\bullet-}$)[6b]—K (k_1/k_{-1} in Scheme 1) is equal to 1.8 × 10^{-8}. Therefore, for the hypothetically reversible case under consideration, k_{-1} would be 1.2/K, or ∼7 × 10^7 M^{-1} s^{-1}. Using these values, eq 7 is evaluated for three cases: $k_2 \gg k_{-1}$, $k_2 \approx k_{-1}$, and $k_2 \ll k_{-1}$.

Case 1. If $k_{-1} \ll k_2$, then k_2 is close to the diffusion limit (10^9−10^{11} M^{-1} s^{-1})[19,33] as expected for Brønsted acid−base reactions. Here, eq 7 reduces to eq 8, and the reaction is independent of [H$^+$].

$$-\mathrm{d}[\mathbf{1}_{1e}]/\mathrm{d}t = k_1[\mathbf{1}_{1e}][O_2] \qquad (8)$$

This is an ETPT mechanism, kinetically indistinguishable from path B, the published ETPT mechanism for reductions of O_2 by $\mathbf{1}_{1e}$, $\mathbf{2}_{1e}$, and $\mathbf{3}_{1e}$ at pH 1.8.[6a,b] Importantly however, both pathways B and C are independent of [H$^+$].

Case 2. If $k_{-1} \approx k_2$, the dependence of rate on [H$^+$] is nonlinear. This is contrary to experimental observation.

Case 3. If $k_{-1} \gg k_2$ (i.e., $k_2 \ll 7 \times 10^7$ M^{-1} s^{-1}), eq 7 reduces to eq 9 (where $K = k_1/k_{-1}$), and path C would display a linear dependence on [H$^+$].

$$-\mathrm{d}[\mathbf{1}_{1e}]/\mathrm{d}t = Kk_2[\mathbf{1}_{1e}][O_2][H^+] \qquad (9)$$

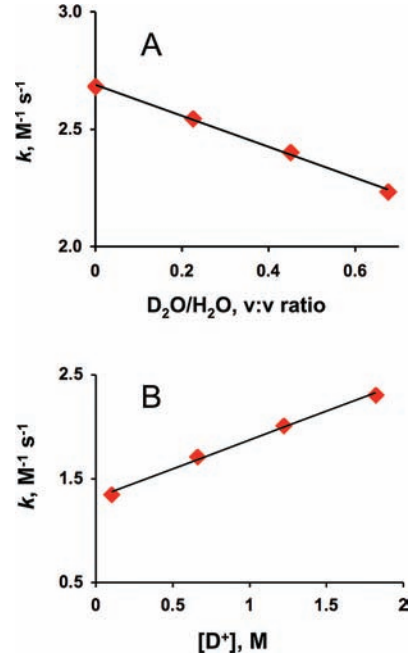

Figure 4. Rate constants, k, as a function of D_2O:H_2O ratios and [D$^+$]. (A) Rate constants as a function of volume percent of D_2O at 1.9 M H$^+$(D$^+$) and constant 2.0 M ionic strength (0.1 M LiCl). (B) Rate constants as a function of [D$^+$] in 75% v:v D_2O:H_2O at 0.1 M LiCl. KIE values from the two methods (panels A and B) are k_{CPET}/k_{CDET} = 1.75 and 1.7, respectively.

This means that, to observe a linear dependence on [H$^+$], the rate constant, k_2, for protonation of $O_2^{\bullet-}$ in ($\mathbf{1}_{ox}$,$O_2^{\bullet-}$) would have to be ≪7 × 10^7 M^{-1} s^{-1} (k_{-1}). This is much too small for a Brønsted acid−base reaction and contrary to experimental data for rates of PT from hydronium ions in bulk water to the conjugate-base forms of weak acids.[19d,f,j] *This rules out path C as a possible source for the linear dependence of rate on [H$^+$].*

This situation is effectively the opposite of the reduction of O_2 by C_{60}^- in the presence of NH_4^+ in organic solvents.[13] There, back-ET, k_{-1}, is nearly diffusion-controlled, and PT from NH_4^+ to $O_2^{\bullet-}$ is encumbered by the need to break an N−H bond. Finally, while some POMs, such as the 2e$^-$-reduced anion $H_2SiW_{12}O_{40}^{4-}$, can slowly reduce H$^+$, control experiments (see Materials and Methods) rule out H$^{\bullet}$ as an intermediate in the proton-coupled reduction of O_2 to $HO_2^{\bullet}$ by $\mathbf{1}_{1e}$.

The above analysis is the first of several lines of evidence that the first-order dependence of rates on [H$^+$] in Figure 3 is due to a linear combination of path B (ETPT) and path A (CPET). The CPET reaction is first-order in all three reactants, $\mathbf{1}_{1e}$, O_2, and H$^+$ (eq 10).

$$-\frac{1}{2}\mathrm{d}[\mathbf{1}_{1e}]/\mathrm{d}t = (k_{ET} + k_{CPET}[H^+])[\mathbf{1}_{1e}][O_2] \qquad (10)$$

The y-intercept and slope of the line in Figure 3 give k_{ET} = 1.17 M^{-1} s^{-1} and k_{CPET} = 0.80 M^{-2} s^{-1}. As predicted by Krishtalik[34] and Savéant,[10d] the CPET rate constant is independent of pH, while rates vary with [H$^+$], which is present as a reactant.

Kinetic Isotope Effects. Kinetic isotope effect (KIE) data were obtained in two ways. In the first (Figure 4A), the volume-volume ratio of D_2O to H_2O was varied at a constant concentration of 1.9 M added HCl. The rate constant for the D$^+$-dependent

(32) Duncan, D. C.; Hill, C. L. *J. Am. Chem. Soc.* **1997**, *119*, 243–244.
(33) (a) Jordan, R. B. *Reaction Mechanisms of Inorganic and Organometallic Systems*, 3rd ed.; Oxford University Press: New York, 2007. (b) Herzig, M.; Knoche, W. *J. Phys. Chem. A* **1998**, *102*, 1304–1308. (c) Kim, Y. N. *Phys. Rev. Lett.* **1968**, *20*, 359–360.
(34) Krishtalik, L. I. *Biochim. Biophys. Acta* **2003**, *1604*, 13–21.

pathway, k_{CDET} (= 0.45 M^{-2} s^{-1}), was then calculated using eq 11, in which x/y is the v:v fraction of D_2O to H_2O. (Equation 11 reveals the effect of the D_2O:H_2O v:v ratio on the rate constant for the concerted D^+-ET pathway.) The KIE was k_{CPET}/k_{CDET} = 1.75. The linear relationship between rate and mole-fraction of D_2O in Figure 4A has been observed for other CPET reactions,[12d] and is consistent with the transfer of a single proton.[9c]

$$-\frac{1}{2}d[\mathbf{1}_{1e}]/dt = (k_{ET} + yk_{CPET}[H^+] + xk_{CDET}[D^+])[\mathbf{1}_{1e}][O_2] \quad (11)$$

In the second method (Figure 4B), $[D^+]$ was varied from 0.1 to 1.9 M in 75% D_2O, and the data were analyzed using eq 12. (The use of 100% D_2O was impractical, as it would have required bulk electrolysis of $\mathbf{1}_{ox}$ in large volumes of D_2O.)

$$-\frac{1}{2}d[\mathbf{1}_{1e}]/dt = (k_{ET} + 0.25k_{CPET}[H^+] + 0.75k_{CDET}[D^+])[\mathbf{1}_{1e}][O_2] \quad (12)$$

The value of k_{CDET} was 0.48 M^{-2} s^{-1}, substantially smaller than the corresponding value of k_{CPET} measured in 100% H_2O (Figure 3; 0.80 M^{-2} s^{-1}), such that the KIE[35,36] was k_{CPET}/k_{CDET} = 1.7.[37] (At 0.1 M H^+ (D^+), at which CPET is not kinetically significant, the KIE is 0.9 ± 0.1.[12a,15b])

These values are similar to those reported by Savéant[1m,38] for concerted (electrochemical) proton and electron transfer (CPET) to superoxide in organic solvents, with dissolved water as proton donor. There, k_H/k_D values varied from 1.7 to 3 as concentrations of water in acetonitrile increased from 0.3 to 1.0 M. KIE values for both CPET reductions of dioxygen (this work) and of superoxide[1m,38] are also similar to (1) a primary kinetic isotope value of k_{NH}/k_{ND} = 2.3 reported by Roth and Mayer[12a] for multisite HAT between protonated and nonprotonated bi-imidazoline complexes of Fe(III) and Fe(II), (2) KIE values from 1.6 to 2.8 for CPET oxidations of phenols with pendant hydrogen-bonded bases,[39,40] (3) a KIE of 1.6 for CPET oxidation of phenol by triplet C_{60} in the presence of trimethylpyridine (base),[41] and (4) KIE values of 1.5−3 for CPET oxidations of tyrosine by covalently linked tris-bipyridine−ruthenium(III) complexes with water as proton acceptor.[18b] For electrochemical oxidation of phenols coupled with intramolecular amine-driven PT, Savéant observed a mechanistically diagnostic KIE of 1.8.[16c] For the proton-coupled oxidation of an H-bonded tyrosine−phosphate complex by $Os^{III}(bpy)_3^{3+}$, a KIE of 2.1 ± 0.6 was observed.[15b] Also, in certain cases, KIEs for proton/deuteron transfer from photoacids to bulk water[42] and from hydronium ions to acetate[19d] are both 1.5.

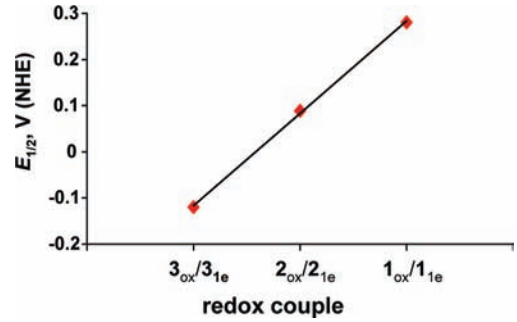

Figure 5. First one-electron reduction potentials of anions from the isostructural series, α-$X^{n+}W_{12}O_{40}^{(9-n)-}$ (X^{n+} = P^{5+}, Si^{4+}, Al^{3+}; $\mathbf{1}_{1e}$, $\mathbf{2}_{1e}$, and $\mathbf{3}_{1e}$) at conditions used in the present work (0.1 M H^+ and 1.9 M LiCl).

Reductions of O_2 by Isostructural Keggin Ions. Additional information was obtained by using α-$Si^{4+}W_{12}O_{40}^{5-}$ ($\mathbf{2}_{1e}$) and α-$Al^{3+}W_{12}O_{40}^{6-}$ ($\mathbf{3}_{1e}$), members of the isostructural series, α-$X^{n+}W_{12}O_{40}^{(9-n)-}$ (X^{n+} = P^{5+}, Si^{4+}, Al^{3+}; $\mathbf{1}_{1e}$, $\mathbf{2}_{1e}$, and $\mathbf{3}_{1e}$). The three ions possess identical crystallographic radii (r = 5.6 Å).[6] As a result, their reduction potentials vary linearly with charge q (i.e., as a linear function of q/r)[20] (Figure 5).

Effect of Gibbs Free Energies of Reaction. The trend in Figure 5 is significant because ET rate constants are predicted to increase more rapidly than competing CPET pathways as Gibbs free energies, $\Delta G°$, become more favorable.[1o,43] From a Marcus model perspective, ET reactions have smaller reorganization energies, λ, so that shifts to more negative (favorable) $\Delta G°$ values result in larger increases in rate constants for ET (and ETPT) than for CPET.[15c,16d]

This was investigated by determining rate constants for reductions of O_2 by $\mathbf{2}_{1e}$. The potential of the $\mathbf{2}_{ox}/\mathbf{2}_{1e}$ couple is 90 mV (vs NHE), while that for the $\mathbf{1}_{ox}/\mathbf{1}_{1e}$ couple is 280 mV. Correspondingly, $\Delta G°$ for ET from $\mathbf{2}_{1e}$ to O_2 (+5.5 kcal mol^{-1}) is significantly more favorable than $\Delta G°$ for ET from $\mathbf{1}_{1e}$ to O_2 (+9.9 kcal mol^{-1}). As shown in Figure 6, rate constants for reactions of $\mathbf{2}_{1e}$ with O_2 remain nearly constant as $[H^+]$ values increase from 0.1 to 1.9 at 2.0 M ionic strength.[44] This should be compared to reactions of $\mathbf{1}_{1e}$ with O_2 (Figure 3), where rate constants increased by a factor of 2.25.[45]

These findings are in line with the expectation that, as Gibbs free energies ($\Delta G°$) become more favorable, k_{ET} should become more kinetically significant than k_{CPET}.[43,46] Conversely, CPET increases in importance as the underlying ET reaction become

(35) The distribution of H^+ and D^+ among H_2O, HDO, and D_2O is influenced by the slightly different relative affinities within each proton(deuteron)/solvent pair, which, in turn, are also affected by the nature and concentration of electrolyte ions (see ref 36). However, because nearly identical KIE values are obtained by two different methods, one involving variation in the D_2O/H_2O v:v ratio (Figure 4A) and the other at a constant D_2O/H_2O v:v ratio (Figure 4B), these effects appear to be small.

(36) (a) Gold, V. *Proc. Chem. Soc.* **1963**, 141–143. (b) Halevi, E. A.; Long, F. A.; Pau, M. A. *J. Am. Chem. Soc.* **1961**, *83*, 303–311. (c) Purlee, E. L. *J. Am. Chem. Soc.* **1959**, *81*, 263–272.

(37) The conditions used to obtain the data in Figure 4B (variable $[H^+]$ at constant 0.1 M LiCl) are similar to those used in control reactions with no added LiCl in Figure 3 (indicated by black diamonds). Those data show that k_{CPET} is statistically identical in the presence or absence of LiCl.

(38) Savéant, J.-M. *J. Phys. Chem. C* **2007**, *111*, 2819–2822.

(39) See ref 12a for a discussion of experimental and theoretical aspects on the wide range of KIE values reported for a variety of proton-coupled electron-transfer reactions. For two reviews of theoretical aspects, see ref 40.

(40) (a) Peters, K. S. *Acc. Chem. Res.* **2009**, *42*, 89–96. (b) Hammes-Schiffer, S. *Acc. Chem. Res.* **2001**, *34*, 273–281.

(41) Biczók, L.; Gupta, N.; Linschitz, H. *J. Am. Chem. Soc.* **1997**, *119*, 12601–12609.

(42) Mohammed, O. F.; Pines, D.; Pines, E.; Nibbering, E. T. *J. Chem. Phys.* **2007**, *341*, 240–257.

(43) (a) Anderson, A. B.; Cai, Y.; Sidik, R. A.; Kang, D. B. *J. Electroanal. Chem.* **2005**, *580*, 17–22. (b) Soudackov, A.; Hammes-Schiffer, S. *J. Chem. Phys.* **2000**, *113*, 2385–2396. (c) Decornez, H.; Hammes-Schiffer, S. *J. Phys. Chem. A* **2000**, *104*, 9370–9384.

(44) The reaction between $\mathbf{2}_{1e}$ and O_2 follows a pathway analogous to B in Scheme 1. For the rate of pathway C to depend on $[H^+]$, the rate constant for protonation of the successor complex ($\mathbf{2}_{ox}$,$O_2^{\bullet-}$)—analogous to ($\mathbf{1}_{ox}$,$O_2^{\bullet-}$) in Scheme 1—would have to be unreasonably small: ≤∼105 M^{-1} s^{-1}.

(45) Control experiments showed that the small increase in rate constants in Figure 6 is due to the effects of slight Li^+ association; see Figure S3 in the Supporting Information for additional kinetic and electrochemical data.

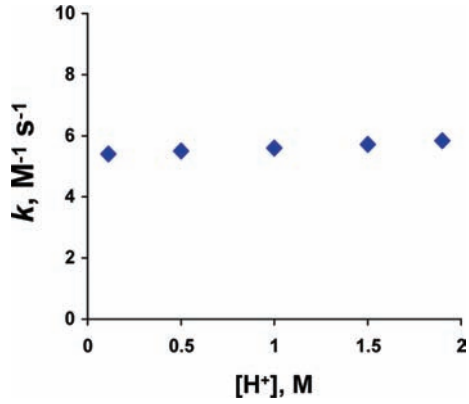

Figure 6. Rate constants for reactions of $\mathbf{2}_{1e}$ with O_2 as a function of $[H^+]$ at constant ionic strength (2.0 M by addition of LiCl).

more *endergonic*. This is important in light of the recent identification of superoxide as an intermediate in the oxygen reduction reaction (ORR) at Pt under alkaline conditions[1j,k] and (notably) by Bi-modified Au electrodes under *acidic* conditions.[1n] For the ORR in *acidic* conditions, as actually prevail in many fuel cells, Anderson has predicted that, as electrode overpotentials *decrease* (a goal in fuel-cell research), CPET should become more kinetically (and practically) significant.[1o,43a]

Reduction of O_2 by a Deliberately Protonated Keggin Ion Electron Donor. Next, α-$AlW_{12}O_{40}^{6-}$ ($\mathbf{3}_{1e}$) was used as an electron donor. Due to its large negative charge, $\mathbf{3}_{1e}$ is significantly protonated at $[H^+]$ values larger than 0.1 M. Taking advantage of this, $\mathbf{3}_{1e}$ was deliberately protonated prior to reaction with O_2. This was done to determine whether the presence of a proton in the inner coordination/solvation environment of the electron donor might dramatically enhance the rate of CPET. This is conceptually analogous to the use of *internal* bases to *accept* protons in intramolecular CPET oxidations of phenols tethered to pendant amine groups.[10a,16c,d]

Protonation of $\mathbf{3}_{1e}$ as a function of $[H^+]$ was quantified by CV at constant ionic strength (Figure S7, Supporting Information) and with no electrolyte other than HCl (Figure 7A). As $[H^+]$ values increase, reduction potentials move to more positive values, a clear indication that reduction of $\mathbf{3}_{ox}$ to $\mathbf{3}_{1e}$ is accompanied by protonation, as shown in eq 13, where K_{assoc} is the constant for H^+ association.

$$\alpha\text{-}AlW_{12}O_{40}^{5-}(\mathbf{3}_{ox}) + e^- + H^+ \overset{K_{assoc}}{\rightleftharpoons} \alpha\text{-}HAlW_{12}O_{40}^{5-}(H\mathbf{3}_{1e}) \quad (13)$$

The association constant, K_{assoc}, was determined from the Nernstien dependence of $E_{1/2}$ on $[H^+]$ in Figure 7A.[29b,47] Fitting of the data to an equation[48] describing this dependence (solid curve in Figure 7A) gives $K_{assoc} = 1.4 \pm 0.5\ M^{-1}$, indicative of substantial H^+ association (e.g., at 0.7 M H^+, 50% of the $\mathbf{3}_{1e}$ anions are present as $H\mathbf{3}_{1e}$). Electrochemical evidence for

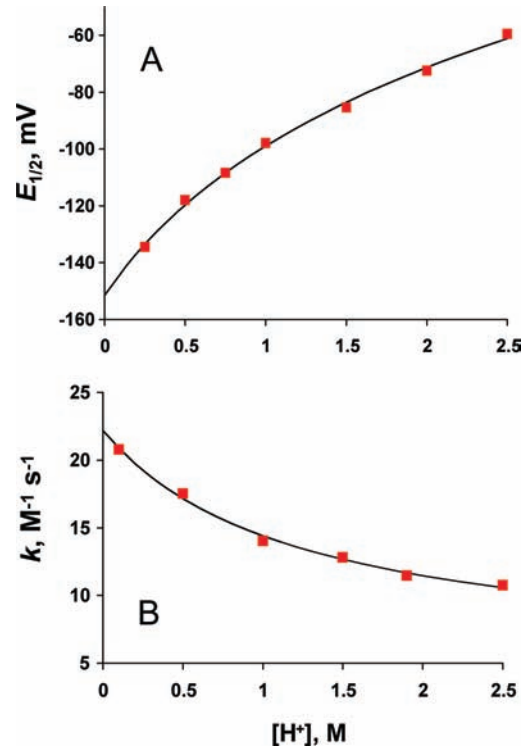

Figure 7. Reduction potentials for the $\mathbf{3}_{ox}/\mathbf{3}_{1e}$ couple (A) and rate constants for reactions of $\mathbf{3}_{1e}$ with O_2 (B) as functions of $[H^+]$ in the absence of added LiCl.

association of a second proton, to give $H_2\mathbf{3}_{1e}$, is observed at $[H^+]$ values larger than 3 M.

Rate constants were then obtained as a function of $[H^+]$ (from 0.1 to 1.9 M) with no added LiCl. As shown in Figure 7B, rate constants now *decrease* with $[H^+]$. This is consistent with the shift in reduction potentials of the $\mathbf{3}_{ox}/\mathbf{3}_{1e}$ couple to more positive values with increase in $[H^+]$ (Figure 7A), which makes ET to O_2 *less* energetically favorable. More quantitatively, the functional dependence of rate constants, k, on $[H^+]$ (fitted curve in Figure 7B)[29b] gives $K_{assoc} = 0.8 \pm 0.2\ M^{-1}$, within experimental uncertainty of the K_{assoc} value ($1.4 \pm 0.5\ M^{-1}$) obtained from the CV data in Figure 7A.[48] This confirms that the decrease in rate constants with $[H^+]$ in Figure 7B is correctly attributed to protonation of $\mathbf{3}_{1e}$. Rather than an increase in rate that might be attributed to more facile CPET by protonated $\mathbf{3}_{1e}$,[49] apparent rate constants decrease with increasing $[H^+]$. At the same time, the *nonlinear*

(46) See the Supporting Information for a discussion of issues involved in the identification of heteropolyanion electron donors with reduction potentials more *positive* than that of the $\mathbf{1}_{ox}/\mathbf{1}_{1e}$. One candidate, for which rate data are provided in the Supporting Information, is the one-electron-reduced Wells−Dawson ion, α-$P_2W_{18}O_{68}^{7-}$ ($\mathbf{4}_{1e}$). Unfortunately, this anion is significantly protonated at $[H^+]$ values larger than 0.1 M.

(47) Grigoriev, V. A.; Hill, C. L.; Weinstock, I. A. *J. Am. Chem. Soc.* **2000**, *122*, 3544–3545.

(48) The functional dependence of $E_{1/2}$ on $[H^+]$ is

$$E_{1/2} = E_\circ + \frac{RT}{nF}\ln\left(\frac{1 + K_{red}(\gamma_H\gamma_{red}/\gamma'_{red})[H^+]}{1 + K_{ox}(\gamma_H\gamma_{ox}/\gamma'_{ox})[H^+]}\right) + \frac{RT}{nF}\ln\frac{\gamma_{ox}}{\gamma_{red}}$$

where "red" and "ox" refer to the fully oxidized and one-electron-reduced forms of the electron-accepting POM anion. In the present case, the fully oxidized anion, $\mathbf{3}_{ox}$, has the same charge as that of $\mathbf{2}_{1e}$ (5− for both). Based on the CV and kinetic data in Figure S3, $\mathbf{3}_{ox}$ is only slightly protonated as $[H^+]$ values increase from 0.1 to 1.9 M (i.e., $K_{ox} \ll 1$). Hence, the dependence of $E_{1/2}$ on $[H^+]$ can be approximated by the first two terms in the series expansion, $E_{1/2} = E^\circ + a\ \ln(1 + K_{red}[H^+])$, in which E°, a, and K_{red} are adjustable parameters. Fitting of the data in Figure 7A gives $E^\circ = -151$ mV and $K_{red} = 1.4 \pm 0.5$.

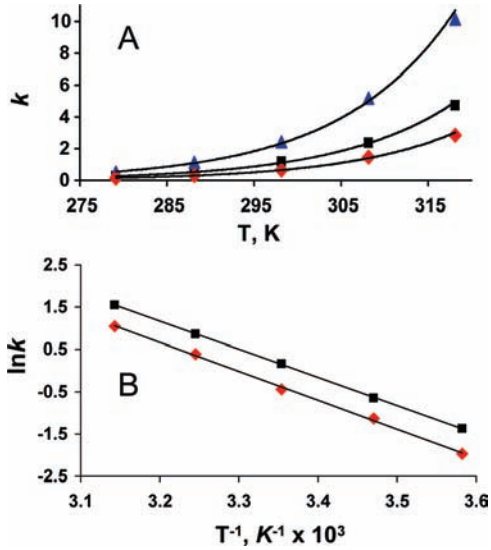

Figure 8. Activation parameters. (A) Rate constants (M^{-1} s^{-1}) as a function of temperature at $[H^+] = 0.1$ (black squares) and 1.9 M (blue triangles). At each temperature, rate constants, k_{CPET}, for the CPET pathway (red diamonds, M^{-2} s^{-1}) were calculated by subtracting k_{ET} values obtained at 0.1 M H^+ from composite rate constants obtained at 1.9 M H^+ (i.e., $k_{CPET} = (k - k_{ET})/[H^+]$). (B) Ahrrenius plots (ln k vs T^{-1}) for the k_{ET} and k_{CPET} values obtained from the data in panel A.

decrease caused by deliberate protonation of $\mathbf{3}_{1e}$ provides an additional line of evidence that hydronium ions in *bulk water* (i.e., not preassociated with $\mathbf{1}_{1e}$) are responsible for the *linear* dependence of rate on $[H^+]$ in Figure 3.

Temperature Dependence of ET and CPET. To obtain activation parameters associated with the CPET rate constant, k_{CPET}, the temperature dependence of the reaction between $\mathbf{1}_{1e}$ and O_2 was determined at constant ionic strength at two $[H^+]$ values. At 0.1 M H^+, the CPET pathway is not kinetically significant (at 298 K, $k_{CPET}[H^+] = 0.08$ M^{-1} s^{-1}), such that the temperature dependence is that of k_{ET} (black squares in Figure 8A). At 1.9 M H^+, CPET is competitive with ET (at 298 K, $k_{ET} = 1.2$ M^{-1} s^{-1} and $k_{CPET}[H^+] = 1.5$ M^{-1} s^{-1}). The sum of these rate constants, k ($= k_{ET} + k_{CPET}[H^+]$), was determined as a function of temperature at 1.9 M H^+ (blue triangles in Figure 8A), and the temperature dependence of k_{CPET} (red diamonds in Figure 8A) was then obtained by subtracting k_{ET} values at each temperature. Hammarström used an analogous subtraction method to determine the temperature dependence of rate constants associated with the CPET oxidation of TyrOH in the presence of a parallel ET pathway.[15c]

Activation Parameters for ET and CPET. The Marcus model provides a useful starting point for evaluating the temperature dependence of rate constants for parallel ET and CPET pathways. If the temperature dependence of $\Delta G°$ is small, activation energies, E_a, from slopes of the Arrhenius plots of ln k_{ET} and ln k_{CPET} versus T^{-1} (Figure 8B) can be evaluated using eqs 14−16, where A (the y-intercept) is the total pre-exponential factor, λ is the reorganization energy, and H_{RP} is the reactant−product electronic-state coupling constant.

$$k = A\, e^{-E_a/k_B T} \tag{14}$$

$$E_a = \frac{(\lambda + \Delta G°)^2}{4\lambda} \tag{15}$$

$$A = \frac{2\pi}{\hbar}\frac{{H_{RP}}^2}{\sqrt{4\pi\lambda RT}} \tag{16}$$

The nearly parallel lines in Figure 8B give similar activation energies, $E_a = 13.2$ and 13.6 kcal mol^{-1}, respectively, for the ETPT and CPET pathways, and the standard Gibbs free energy, $\Delta G°$, for CPET is more favorable than for ET by 6.9 kcal mol^{-1}. These and other parameters, calculated using eqs 15 and 16, are listed in Table 1. Reorganization energies, λ, appear to increase from 30 kcal mol^{-1} (1.3 eV) for ET to 48 kcal mol^{-1} (2.1 eV) for CPET, while the respective coupling constants, H_{RP}, are 5 and 6 cm^{-1}.

The λ and H_{RP} values in Table 1 are remarkably similar to those obtained by analogous methods for the CPET oxidations of tyrosine models[15c] and hydrogen-bonded phenols[16d,f] (see Supporting Information for additional discussion). For both of those classes of reactions, however, differences between calculated λ_{ET} and λ_{CPET} values are considerably smaller when the temperature dependence of $\Delta G°$ is included.[18b,10a] Therefore, activation parameters were also calculated using a form of the Marcus model that takes into account the temperature dependence of the Gibbs free energy as well as possible nonadiabaticity (eqs 17 and 18).[16b]

$$k = \chi Z \exp\left[-\frac{\lambda}{4RT}\left(1 + \frac{\Delta G°}{\lambda}\right)^2 - \frac{\Delta E_{ZP}}{RT}\right] \tag{17}$$

$$Z = N_A d^2 \sqrt{\frac{8\pi RT}{M}} \tag{18}$$

In eq 17, χ is the transmission coefficient, and ΔE_{ZP}, calculated from the experimental value for k_H/k_D, is the difference between the zero-point energies of the transition and reactant states of the transferring proton.[50] The frequency factor, Z, is calculated using eq 18, in which N_A is Avogadro's number, d is the sum of the radii of the electron donor and acceptor, and M is the reduced mass of the reacting species. Substitution of eq 18 into eq 17, replacement of $\Delta G°$ by $\Delta H° - T\Delta S°$, and rearrangement gives the following relationship:

$$\ln\frac{k}{\sqrt{T}} = \ln\left(\chi N_A d^2\sqrt{\frac{8\pi R}{M}}\right) + \frac{\Delta S°}{2R} + \frac{\Delta S°\Delta H°}{2R\lambda} - \frac{\Delta S°^2}{4R\lambda}T - \left(\frac{\lambda}{4R} + \frac{\Delta H°}{2R} + \frac{\Delta H°^2}{4R\lambda} + \frac{\Delta E_{ZP}}{R}\right)\frac{1}{T} \tag{19}$$

Before using eq 19, it was noted that the ET pathway and k_{ET}, extensively studied in previous work,[6a,b] are adiabatic: use of the adiabatic Marcus model to estimate k_{ET} for reaction of $\mathbf{1}_{1e}$ with O_2 gave values of 1.1[6b] and 0.96[6a] M^{-1} s^{-1}, compared with an experimental value[6b] of 1.4 ± 0.2 M^{-1} s^{-1}. Hence, χ_{ET} was set equal to 1.0, and Z (from eq 18) was estimated to be 5.7×10^{11} M^{-1} s^{-1}. This information, along with temperature

(49) A limitation of this experiment is that the driving force, $\Delta G°$, for ET to O_2 from $\mathbf{3}_{1e}$ is 4.5 kcal mol^{-1} more negative than that for ET from $\mathbf{2}_{1e}$, and 9 kcal mol^{-1} more negative than that for ET from $\mathbf{1}_{1e}$. Hence, k_{CPET} is expected to be less kinetically significant here than for ET to O_2 from $\mathbf{2}_{1e}$. Despite this, the data clearly rule out a large enhancement of k_{CPET} upon preassociation of H^+ with the electron donor.

(50) $\Delta E_{ZP} = \ln(k_H/k_D)RT/(1/2^{1/2}-1)$, where k_H/k_D is the KIE associated with the CPET pathway.

Table 1. Parameters Associated with Electron Transfer (ET) and Concerted Proton−Electron Transfer (CPET) Reductions of Dioxygen

pathway	k	$\Delta G^{\circ\prime}$, kcal mol^{-1}	E_a, kcal mol^{-1}	H_{RP}, cm^{-1}	$\Delta S^{\ddagger}$,[c] cal mol^{-1} K^{-1}	λ, kcal mol^{-1}	λ, eV	k_H/k_D
ET	$k_{ET} = 1.2$ M^{-1} s^{-1}	9.9[a]	13.2	5	−14	29.7	1.3	0.9 ± 0.1[d]
CPET	$k_{CPET} = 0.8$ M^{-2} s^{-1}	3.0[b]	13.6	6	−16	48.2	2.1	1.7 ± 0.1[e]

[a] From electrochemical data for the $\mathbf{1}_{ox}/\mathbf{1}_{1e}$ and $O_2/O_2^{\bullet-}$ couples (+0.25 and −0.16 V, respectively, vs NHE), plus 0.43 kcal mol^{-1} from anion−anion repulsion within $[(\mathbf{1}_{ox})(O_2^{\bullet-})]^{4-}$ successor−complex ion pairs. See refs 6a and 6b for details concerning the role of electrostatic work terms in the calculation of ET rate constants. [b] From electrochemical data for the $\mathbf{1}_{ox}/\mathbf{1}_{1e}$ couple and the standard potential of the $O_2/HO_2^{\bullet}$ couple (+0.12 V vs NHE), with no anion−anion repulsion within $[(\mathbf{1}_{ox})(HO_2^{\bullet})]^{3-}$ successor complexes. [c] $\Delta S^{\ddagger}$ values are from Eyring plots (Figure S8, Supporting Information). [d] Experimental values are statistically indistinguishable from unity. The uncertainty is due to determinations of k_H and k_D at 0.1 M $H^+(D^+)$ using slightly different methods and electrolytes (see Materials and Methods). [e] Average of values from two different methods: variation of D_2O:H_2O v:v ratios at a single acid concentration, and variation of $[D^+]$ in 75% D_2O (Figure 4).

dependence data for both the ET and CPET rate constants (Figure 8B) and eq 19, was used to estimate the reorganization energies for both pathways (Figures S9 and S10, Supporting Information). This gave 41.5 and 52.4 kcal mol^{-1}, respectively, for λ_{ET} and λ_{CPET}. (Uncertainty from the nonlinear fitting used to obtain λ_{CPET} gives 52.4 ± 1.5 kcal mol^{-1}.) Hence, when the temperature dependence of ΔG° is included, λ_{CPET} is larger than λ_{ET} by 10.9 ± 1.5 kcal mol^{-1} (0.5 eV).[51]

Unlike for ET, the collision frequency, Z_{CPET}, for CPET cannot be calculated from the relationship in eq 18. That model refers to bimolecular collisions, while the multisite CPET reaction is first-order in three components: $\mathbf{1}_{1e}$, O_2, and H^+. Without knowledge of Z_{CPET}, eq 19 cannot be used to provide a value for the transmission coefficient, χ_{CPET}. This problem was partially overcome by deriving an equation analogous to eq 19 that included the product, $Z_{CPET}\,\chi_{CPET}$ (eq 20). In this derivation, eq 20 was linearized by noting that, for CPET, the quadratic term, $(\Delta G^{\circ}/\lambda_{CPET})^2$, in eq 17 is small (see Table 1). From eq 20, the y-intercept of the plot of ln k_{CPET} vs T^{-1} (Figure S11, Supporting Information) gave $Z_{CPET}\,\chi_{CPET} = 3 \times 10^9$ M^2 s^{-1}. When the uncertainty in this large extrapolation is included (95% confidence intervals), $Z_{CPET}\,\chi_{CPET}$ is estimated to lie between 7×10^8 and 1×10^{10} M^{-2} s^{-1}.

$$\ln k_{CPET} = \ln Z_{CPET}\chi_{CPET} + \frac{\Delta S^{\circ}}{2R} - \frac{\lambda/4 + \Delta H^{\circ}/2 + \Delta E_{ZP}}{R}\frac{1}{T} \tag{20}$$

Finally, although the CPET reaction is first-order in all three components, the probability of a *simultaneous three-body collision* occurring in the condensed phase is small. Moreover, by setting χ_{CPET} to its maximum value of 1, Z_{CPET} ranges from approximately 10^8 to 10^{10} M^2 s^{-1}; these values represent the *smallest possible* collision frequencies for the CPET reaction. These *minimum Z* values are unreasonably large for a (*hypothetical*) simultaneous three-body collision in the condensed phase. This raises an important question regarding the elementary step associated with the multisite CPET to O_2 in water. This is addressed in the Discussion section.

Discussion

Mechanism of Multisite CPET to Dioxygen in Water. Most CPET reactions are intramolecular,[9c,d,12a] bimolecular,[9c,d] or heterogeneous[9a] (i.e., electrochemical) and/or involve the loss of protons to buffer or solvent. For example, intramolecular CPET oxidations of tyrosine models involve chemical oxidations of phenols, simultaneously coupled to PT from phenol to proton acceptors (eq 21, where Ox is the oxidant, and B**:** is a base, such as acetate or solvent).[9c,d]

$$\text{Ox-ArOH} + \text{B:} \rightarrow \text{Red-ArO}^{\bullet} + \text{B:H} \tag{21}$$

In another class of CPET reactions, the electrochemical reduction of $O_2^{\bullet-}$ to HO_2^- in organic solvents that contain small amounts of water, ET to $O_2^{\bullet-}$ is preceded by the formation of hydrogen-bonded $[O_2^{\bullet-}\cdots H_2O]$ complexes (eq 22).[1m,38,52]

$$[O_2^{\bullet-}\cdots H_2O] + e^- \rightarrow HO_2^- + HO^- \tag{22}$$

In all these cases, the proton is initially bound to the site at which oxidation or reduction occurs. This obviates the need for consideration of a three-body collision en route to the transition state for CPET. That is not true, however, for the present multisite CPET to O_2 (eq 23). This reaction is first-order in all three reacting species, which raises a fundamental problem because the simultaneous collision of all three reactants in water not only is implausible but is ruled out by the large collision frequency ($Z_{CPET} > 10^8$ M^2 s^{-1}) estimated from temperature dependence data.

$$\mathbf{1}_{1e} + O_2 + H^+ \rightarrow \mathbf{1}_{ox} + HO_2^{\bullet} \tag{23}$$

For many apparently termolecular reactions, simultaneous three-body collisions are avoided by pre-equilibria involving associations between two of the three reactants. *In the present case, however, enthalpically governed pre-equilibria between $\mathbf{1}_{1e}$, O_2, and/or H^+ are ruled out by control experiments specifically designed to address this point.* Namely, kinetically significant preassociation between H^+ and $\mathbf{1}_{1e}$ is ruled out by CV data and by the linear dependence of CPET rates on $[H^+]$. In fact, the association of protons to isostructural Keggin ions, such as $\mathbf{3}_{1e}$, and to the Wells−Dawson ion, $\mathbf{4}_{1e}$, causes rates of ET to O_2 to *decrease*. Furthermore, due to the weak basicity of dioxygen, protonation of O_2 to give HO_2^+ intermediates (a PTET mechanism) is not kinetically viable: according to Savéant,[10d] PTET is ruled out by the large negative pK_a of HO_2^+. A PTET mechanism is also inconsistent with the observed deuterium KIE of 1.7. Finally, other work has demonstrated that O_2 does not bind to the hexacoordinate W atoms of $\mathbf{1}_{1e}$.[6a,b,25]

Average Distances between Hydronium Ions and Dioxygen. A resolution to this "three-body" problem emerges by noting that, at the H^+ concentrations at which CPET is observed, the average distances between O_2 molecules and H^+ ions are relatively short (Figure S12, Supporting Information). For example, at 1 M H^+, any O_2 molecule in solution is no farther than 7.3 Å from the

(51) Similar results were obtained when the calculations leading to this result were done starting from reasonably adiabatic χ_{ET} values of 0.75 and 0.5 for outer-sphere ET from $\mathbf{1}_{1e}$ to O_2. For $\chi_{ET} = 0.75$, values of 40.8 and 51.8 kcal mol^{-1} were found for λ_{ET} and λ_{CPET}, respectively; for $\chi_{ET} = 0.50$, values of 39.8 and 50.7 kcal mol^{-1} were found for λ_{ET} and λ_{CPET}.

(52) Singh, P. S.; Evans, D. H. *J. Phys. Chem. B* **2006**, *110*, 637–644.

nearest H^+ ion; at 2 M H^+, this distance decreases to 5.8 Å.[53] These short distances are significant because in kinetic models for proton diffusion in water, calculated "reaction distances" are approximately 2−3 hydrogen bonds, or 6 ± 1 Å.[19j,42,54] These same distances may also allow for the coupling of electron−proton vibronic states necessary for CPET.[10b] This general situation was evaluated in more detail by assessing the fractions of diffusional encounters between $\mathbf{1}_{1e}$ and O_2 that occur within specific distances from H^+ and by determining how these fractions vary as a function of $[H^+]$.

The average number of protons P present within each spherical volume of solution of radius r is given by eq 24.[55,56] As seen by inspection, P increases linearly with $[H^+]$.

$$P = \frac{4}{3}\pi r^3 N_A[H^+] \qquad (24)$$

Next, molecules of O_2 (present at ca. 1 mM) are arbitrarily placed at the center of a small fraction of these spherical volumes. Upon diffusional approach of $\mathbf{1}_{1e}$ to O_2, P is the number of protons within a given radius, r, from O_2 in the $(\mathbf{1}_{1e},O_2)$ encounter pairs. If P is less than unity, then P may be viewed as the fraction of O_2 molecules within a distance r from H^+. If P is larger than unity, this simply means that more than one proton is within a distance r from O_2.

To illustrate this, a $(\mathbf{1}_{1e},O_2)$ encounter pair, with the O_2 molecule located at a 6 Å "reaction distance" from H^+, is drawn to scale in Figure 9A. In Figure 9B, P is plotted as function of $[H^+]$ for hypothetical reaction distances of r = 5, 6, and 7 Å. These values were chosen because they correspond to the range of "reaction distances" ($r = 6 \pm 1$ Å) associated with proton "hopping" in models of proton diffusion.[19]

The plots in Figure 9B reveal that significant fractions of encounters between $\mathbf{1}_{1e}$ and O_2 occur within a range of plausible PT reaction distances r from H^+. In addition, the fraction of $(\mathbf{1}_{1e},O_2)$ encounter pairs that form within each reaction distance (5, 6, and 7 Å from H^+) increases linearly with H^+ concentration.[57] This begins to explain why the CPET pathway can be formally "termolecular" without the need for a three-body collision: *diffusional encounters between* $\mathbf{1}_{1e}$ *and* O_2 *simply occur in close proximity to* H^+. If CPET were diffusion-controlled,[56] the linear relationship in Figure 9B might be

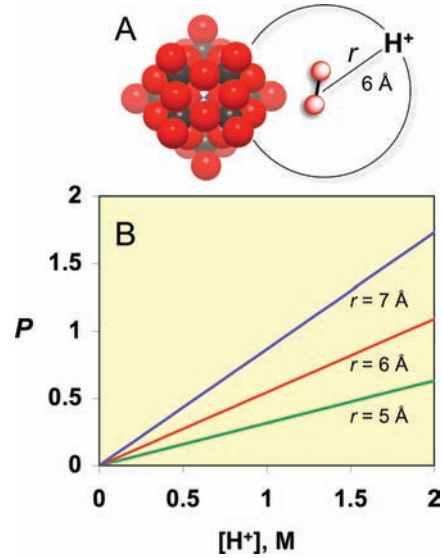

Figure 9. Numbers of protons within spherical volumes of radius r that contain $(\mathbf{1}_{1e},O_2)$ encounter pairs. (A) Scale rendering of a $(\mathbf{1}_{1e},O_2)$ encounter pair (space-filling models), with the O_2 molecule located at a distance of r = 6 Å from H^+. (B) Average numbers of H^+ ions present within specific radii r from O_2, plotted as a function of $[H^+]$ for r = 5 (green line), 6, and 7 Å (blue line). The relative positions of the electron donor, $\mathbf{1}_{1e}$, are not included in the model, but see below for information about the "lifetimes" of the $(\mathbf{1}_{1e},O_2)$ pairs.

sufficient to give a first-order dependence of rate on $[H^+]$. However, both ET and CPET pathways are activation-controlled[58] (rate constants for each are relatively small), and the first-order dependence on $[H^+]$ can only be understood by considering the lifetimes of the $(\mathbf{1}_{1e},O_2)$ encounter pairs.

$(\mathbf{1}_{1e},O_2)$ Encounter Pairs and Proton Diffusion. The result in Figure 9 is purely analytical and includes no assumptions regarding the lifetimes of the $(\mathbf{1}_{1e},O_2)$ encounter pairs. However, hydronium ion diffusion in water is sufficiently rapid that even relatively short encounter-pair lifetimes could significantly increase the probability of CPET. These lifetimes were estimated by calculating the rate constants k_e for diffusional "escape" of $\mathbf{1}_{1e}$ and O_2 from $(\mathbf{1}_{1e},O_2)$ encounter pairs. At 298 K, calculated k_e values ranged from 5×10^9 to 1.4×10^{10} s^{-1}, which give encounter-pair lifetimes τ = 70−200 ps (where $\tau = 1/k_e$).[60−62]

(53) The number of protons within a spherical volume of radius r is $\int_0^r N_A[H^+]4\pi r^2\,dr$. Setting this equal to unity (one H^+ per spherical volume) and integrating from the origin (center of the sphere) to the surface of each spherical volume, one obtains the functional dependence of r on $[H^+]$ as $r = 1/((4/3)\pi N_A[H^+])^{1/3}$. See Figure S12 (Supporting Information) for a plot of $k_{CPET}[H^+]$ values as a function of r.

(54) Bell, R. P. *The Proton in Chemistry*; Chapman & Hall: London, 1973.

(55) This is a modification of the approach used by Czapski and Peled[56] to explain the anomalously small yields of solvated electrons, e^-_{aq}, observed after radiolysis in concentrated solutions of electron scavengers, S. They argued that as concentrations of S increased from 0.1 to 3 M, it became progressively more likely that electrons would be generated in solution as "initially formed" (e^-_{aq}, S) encounter pairs, thus obviating the need for diffusion-controlled encounters between e^-_{aq} and S.

(56) Czapski, G.; Peled, E. *J. Phys. Chem.* **1973**, *77*, 893–897.

(57) This result should be compared to rapid PT from photoacids to acetate anions in water. At acetate concentrations ≥1 M, "reaction distances" from one to five intervening water molecules are observed; acetate *diffusion* no longer plays a significant role (see works by Pines, Nibbering, and Bakker in ref 19). In the present work, H^+ concentrations of ∼1 M are sufficient to ensure that a large fraction of encounters between $\mathbf{1}_{1e}$ and O_2 occur within the accepted values of 6 ± 1 Å[19j,42,54] for the Eigen−Weller "reaction distance" a for PT between acids and bases. Nevertheless, the two cases are fundamentally different: The photoacid reactions are diffusion-controlled, while the present CPET to O_2 is activation-controlled.

(58) The fraction of encounter pairs that proceeds to products can be approximated as the ratio of the rate constants for ET or CPET, which are both close to 1, divided by the collision frequency, Z (10^{11} M^{-1} s^{-1}), or ∼$1/10^{11}$. Because ET and CPET are both activation-controlled, the k_{ET} and k_{CPET} values reported in the Results section are "long-time-scale" rate constants;[59] i.e., they refer to activation-controlled reactions of the $(\mathbf{1}_{1e},O_2)$ encounter pairs.

(59) (a) Harris, J. D.; Oelkers, A. B.; Tyler, D. R. *J. Am. Chem. Soc.* **2001**, *129*, 6255–6262. (b) Noyes, R. M. *J. Am. Chem. Soc.* **1956**, *78*, 5486–5490.

(60) The larger rate constant (and smaller τ value) was calculated using Eigen's treatment of the diffusional separation of encounter pairs:[61]

$$k_e = \frac{k_b T}{2\pi\eta}\frac{1}{R^2}\left(\frac{1}{r_A}+\frac{1}{r_B}\right)\frac{\exp[w(R,\mu)/k_bT]}{R\int_R^\infty r^{-2}\exp[w(r,\mu)/k_bT]\,dr}$$

Here, k_b is the Boltzmann constant, r_A and r_B are molecular radii (1.33 and 5.6 Å for O_2 and $\mathbf{1}_{1e}$, respectively), η is the solvent viscosity, and $w(R,\mu)$ is the usual electrostatic work term from Debye−Hückel theory, where μ is ionic strength. In our system, $w(R,\mu) = 0$ due to the zero charge of the neutral component (O_2) in the encounter complex. The smaller rate constant (for which τ = 200 ps) was calculated using $k_e = D/R^2$,[62] where D is the sum of the diffusion coefficients of both species and R is the sum of their radii (6.93 Å).

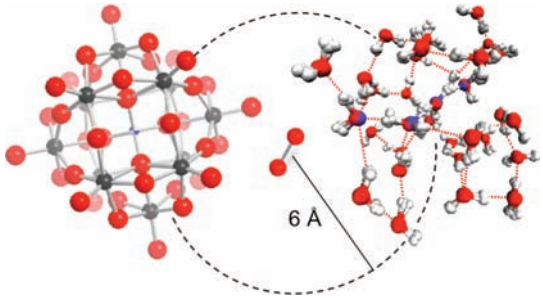

Figure 10. Formation of a ($\mathbf{1}_{1e}$,O_2) encounter pair (lifetime of 70−200 ps) close to an 11-Å-diameter fluxional hydrated-proton complex (far right; ball-and-stick structures are drawn to scale). As drawn, the dioxygen molecule is 6 Å from the positively charged "defect" initially located at the center of the hydrated-proton complex. There is a non-negligible probability for this defect becoming "quantum mechanically delocalized" to within 1 or 2 Å of O_2, an event that occurs within a small fraction of the 70−200 ps lifetime of the ($\mathbf{1}_{1e}$,O_2) pairs. The oxygen atoms over which the protonic defect is delocalized (from center left to upper right) are indicated by a partial covering of blue, which reflects the quantum mechanically probabilistic nature of the delocalization.[19a,h,65]

These lifeteimes are in line with τ values for encounter pairs between molecules and molecular ions in water and organic solvents, which typically range from 10 to 1000 ps.[63]

The estimated lifetime of the ($\mathbf{1}_{1e}$,O_2) encounter pairs is much longer than the time required for protons to diffuse from their average positions to O_2. For example, at 1.0 M H^+, 87% of O_2 molecules in solution lie within 7 Å from an H^+ ion (Figure 9B). If the reaction distance for PT in CPET (i.e., when coupled to ET) is shorter than 7 Å, the 70−200 ps lifetime of the ($\mathbf{1}_{1e}$,O_2) encounter pairs allows ample time for protons to diffuse closer to O_2 before cage escape. Notably, experimental measurements of proton diffusion rates[19j,64a] indicate that only 1.5 ps is required for proton dislocation over a single water molecule (i.e., a distance of ca. 2.5 Å).[64b] In studies of PT from photoacids to proton acceptors, ca. 1.2 ps is required for proton conduction over a single water molecule.[19d,f] Similarly, in theoretical models based on quantum nuclear path-integral simulations, positively charged "defects" can become delocalized over ∼4−5 Å in roughly 10% of the configurations sampled, due mainly to zero-point effects on the PT free-energy profile.[19a,g,h]

This quantum-mechanical situation is depicted in Figure 10, which shows a ($\mathbf{1}_{1e}$,O_2) encounter pair immediately after its formation by diffusional collision. The dioxygen molecule is positioned at a distance of 6 Å from a positively charged "defect", initially located at the center of the ca. 11-Å-diameter fluxional hydrated-proton complex[19a,h,65] (at right in the figure). The blue-labeled oxygen atoms within this complex trace a representative ∼5 Å quantum delocalized path showing the charge defect spread over four hydrogen-bonded oxygen atoms

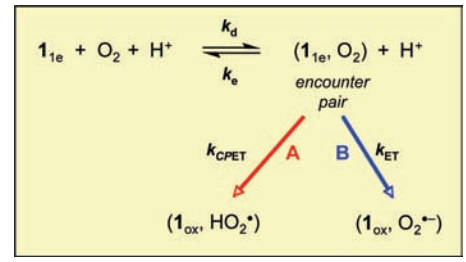

Figure 11. Elementary steps for ET and CPET. Both reactions proceed via the formation of encounter pairs ($\mathbf{1}_{1e}$,O_2). These form by diffusion at a rate equal to the bimolecular collision frequency, Z, estimated from eq 18 at 5.7×10^{11} M^{-1} s^{-1} (k_d), and dissociate from one another with a "cage-escape" rate constant, k_e, estimated at 5×10^9−1.4×10^{10} s^{-1} (which give lifetimes from 70 to 200 ps). At large [H^+], kinetically significant fractions of the ($\mathbf{1}_{1e}$,O_2) encounter pairs form in close proximity to rapidly diffusing H^+ ions, and rates for CPET (k_{CPET}[H^+]) become competitive with those for ET (k_{ET}).

(from center to periphery). Such a path is interpreted as the defect's probing (through thermal and quantum fluctuations) the most likely site in the hydrogen-bond network for the next PT event. The suggestion of such paths is that, within a small fraction of the 70−200 ps lifetime of the ($\mathbf{1}_{1e}$,O_2) encounter pairs, the proton can diffuse to within 1 or 2 Å from O_2.

Taken together, the lifetimes of the ($\mathbf{1}_{1e}$,O_2) encounter pairs, combined with the short distances between O_2 and H^+ and rapid proton mobility, provide multiple opportunities for the three reactants (and solvent) to achieve the positions and energies associated with the transition state for CPET.

Elementary Step in Multisite CPET to O_2. Nevertheless, the rate constant for CPET, k_{CPET}, is orders of magnitude smaller than the rate constant for cage escape, k_e (Figure 11).

Using a steady-state approximation and $k_{CPET}[H^+] \ll k_e$, the rate expression for CPET[66] reduces to eq 25.

$$-\frac{1}{2}\mathrm{d}[\mathbf{1}_{1e}]/\mathrm{d}t = (k_d/k_e)k_{CPET}[\mathbf{1}_{1e}][O_2][H^+] \qquad (25)$$

As a result, CPET is first-order in [H^+] (Figure 3), and the reaction is formally termolecular (eq 10). However, CPET is observed only when $k_{CPET}[H^+]$ becomes similar in magnitude to k_{ET}. For highly endergonic ET reactions such as that of $\mathbf{1}_{1e}$ with O_2, k_{ET} is relatively small, and $k_{CPET}[H^+]$ (CPET) is readily discernible.

Conclusions

Kinetic Data. Data provided here reveal a concerted proton−electron transfer (CPET) pathway for the one-electron

(61) (a) Yoshimura, A.; Md. Uddin, J.; Amasaki, N.; Ohno, T. *J. Phys. Chem. A* **2001**, *105*, 10846–10853. (b) Chiorboli, C.; Indelli, M. T.; Scandola, M. A. R.; Scandola, F. *J. Phys. Chem.* **1988**, *92*, 156–163. (c) Eigen, M. *Z. Phys. Chem.* **1954**, *1*, 176–200.

(62) (a) Stickrath, A. B.; Carroll, E. C.; Dai, X.; Harris, D. A.; Rury, A.; Smith, B.; Tang, K. C.; Wert, J.; Sension, R. J. *J. Phys. Chem. A* **2009**, *113*, 8513–8522. (b) Bagdasaryan, K. S. *Russ. Chem. Rev.* **1984**, *53*, 623–639.

(63) References 61a and 61b list values of 170−2300 and 100−200 ps, respectively, for caged pairs in water. In the following references, values of 250−1000 and 20−55 ps are reported for water and for organic solvents, respectively: (a) Hoffman, M. Z. *J. Phys. Chem.* **1988**, *92*, 3458–3464. (b) Olmsted, J., III; Meyer, T. J. *J. Phys. Chem.* **1987**, *91*, 1649–1655.

(64) (a) Meiboom, S. *J. Chem. Phys.* **1961**, *34*, 375–88. (b) Agmon, N. *Chem. Phys. Lett.* **1995**, *244*, 456–462.

(65) In the quantum path integral used to calculate this structure, typically 8−16 replicas of the system are created (8 replicas are used in Figure 10), and the configurations of these replicas are sampled according to the rules of quantum statistical mechanics. Each quantum configuration is a collection of these replicas. The figure is generated by querying each replica regarding which oxygen atom in that replica is the center of the hydronium ion. The result of this query can differ between replicas, and to indicate which is an hydronium oxygen and which is a water oxygen, two different colors are used, blue and red. The fact that the blue only partially covers the oxygen atoms shows that in the chosen quantum configuration used for the figure, any given oxygen can be both a water oxygen (red) and a hydronium oxygen (blue) simultaneously; i.e., the same oxygen in different replicas can be fundamentally different: water vs hydronium. This results in the "janus-faced" (red and blue) nature of the oxygen atoms along the protonic defect.

(66) While the analysis provided in conjunction with Scheme 1 (Results section) demonstrates that the first-order dependence on [H^+] in Figure 3 is *not* due to rapidly reversible electron transfer from $\mathbf{1}_{1e}$ to O_2, the elementary steps of CPET were left undefined. Clearly, however, both ET and CPET proceed via ($\mathbf{1}_{1e}$,O_2) encounter pairs, as shown in Figure 11.

reduction of dioxygen (O_2) to the protonated superoxide radical ($HO_2^{\bullet}$) by the one-electron-reduced heteropolyanion, α-$PW_{12}O_{40}^{4-}$ ($\mathbf{1}_{1e}$), in water. At modest [H^+] values from 0.01 to 0.10 M, the reduction of O_2 by $\mathbf{1}_{1e}$ occurs via rate-limiting outer-sphere electron transfer, to give the superoxide radical anion ($O_2^{\bullet-}$), which reacts rapidly with H^+ (an ETPT mechanism). From 0.30 to 1.9 M H^+, reaction rates increase linearly with [H^+] due to a previously unknown multisite CPET pathway that involves PT from hydronium ion in bulk water.

These conclusions are supported by (1) a first-order dependence of rate on [H^+], in which H^+ is involved as a reactant; (2) CV data which show that $\mathbf{1}_{1e}$ is not protonated over the range of [H^+] values used; (3) effectively identical [H^+]-dependent rates at constant and variable ionic strengths (to rule out cation association with $\mathbf{1}_{1e}$); (4) the quantitative evaluation of rate expressions for possible mechanisms, from which only CPET results in a linear dependence on [H^+]; (5) definitive and nearly identical deuterium KIEs when the D_2O/H_2O v:v ratio is varied at constant acid concentration, and when [D^+] is varied at constant (75%) D_2O; (6) a modest increase in reorganization energy, from 41.5 to 52.4 kcal mol^{-1}, as the mechanism changes from ET to CPET; (7) a decrease in the relative significance of CPET versus ET pathways as the driving force for ET to O_2 becomes more favorable (by using α-$SiW_{12}O_{40}^{5-}$ ($\mathbf{2}_{1e}$) as the electron donor); and (8) rate *retardation* upon deliberate protonation of α-$AlW_{12}O_{40}^{6-}$ ($\mathbf{3}_{1e}$), which further argues against preassociation of H^+ with $\mathbf{1}_{1e}$ in CPET to O_2.

Elementary Step in CPET to O_2. At the H^+ concentrations at which CPET become competitive with ET, significant fractions of ($\mathbf{1}_{1e}$,O_2) encounter pairs form spontaneously at distances of 6 ± 1 Å from the average positions of "excess" H^+ ions (Figure 9). In models for proton diffusion in water, this value (6 ± 1 Å) is the "reaction distance" for proton "hopping" and is probably within a few angstroms of the "reaction distance" needed for CPET. Moreover, the 70−200 ps lifetimes of the ($\mathbf{1}_{1e}$,O_2) pairs provide ample time for protons to diffuse even closer to O_2 (Figure 10). The overall reaction is first-order in [H^+] because "cage escape", k_e, from the ($\mathbf{1}_{1e}$,O_2) encounter pairs (Figure 11) is orders of magnitude faster than rate-limiting CPET (k_{CPET}). As a result, the rate expression for CPET reduces to $-(1/2)d[\mathbf{1}_{1e}]/dt = (k_d/k_e)k_{CPET}[\mathbf{1}_{1e}][O_2][H^+]$, where k_d is the rate constant for the formation of ($\mathbf{1}_{1e}$,O_2) encounter pairs.

With respect to its coupled proton-transfer step, the herein described multisite CPET is similar to the microscopic reverse of CPET tyrosine (TyrOH) oxidations that involve PT to bulk water. In those reactions, *rate constants* vary with [H^+]. That finding is attributed to the pH-dependent potential of the $TyrO^{\bullet}$/$TyrO^-$ redox couple and the effect of this on the Gibbs free energy for reaction. That fully documented[10c,18c] experimental result is contrary to expectations derived from first principles of thermodynamics. There, rigorous treatments[10d,34] show that rate constants k should be pH-*independent* but that reaction rates should increase linearly with [H^+], with H^+ involved as a reactant. The linear dependence of rates on [H^+] in the present CPET to O_2 is consistent with that expectation.

Implications. The findings provided here introduce a fundamentally new type of CPET reaction involving the chemistry of dioxygen in water. Its novel mechanism emerges from detailed analysis of the elementary steps responsible for the simultaneous coupling of $\mathbf{1}_{1e}$, O_2, and H^+, which is facilitated by the relatively long lifetimes of ($\mathbf{1}_{1e}$,O_2) encounter pairs, in combination with the unique properties of the hydrated "excess" proton in water.

As noted above, reactions of the isostructural Keggin ion donors, α- $X^{n+}W_{12}O_{40}^{(9-n)-}$ ($X^{n+} = P^{5+}$ ($\mathbf{1}_{1e}$) and Si^{4+} ($\mathbf{2}_{1e}$)), provide support for conclusions from computational studies regarding the relationship between CPET and Gibbs free energies, $\Delta G°$. Hammes-Schiffer[43b,c] concludes that, as underlying ET reactions become more endergonic, parallel CPET pathways increase in importance, while Anderson[1o,43a] similarly argues that, as electrode overpotentials *decrease* (a goal in fuel-cell research), CPET should become more kinetically significant.

This relationship between Gibbs free energy and the relative kinetic significance of CPET versus ET pathways has important implications for the redox chemistry of O_2 in water. Namely, in neutral or mildly acidic conditions (pH 1.8 and above), the one-electron-reduced Keggin complexes, α-$X^{n+}W_{12}O_{40}^{(9-n)-}$ ($X^{n+} = P^{5+}$, Si^{4+}, and Al^{3+}; $\mathbf{1}_{1e}$, $\mathbf{2}_{1e}$, and $\mathbf{3}_{1e}$), all reduce O_2 via well-established outer-sphere (ET or ETPT) mechanisms.[6a,b] CPET is observed only for the more endergonic reduction of O_2 by $\mathbf{1}_{1e}$, and only at large H^+ values. This suggests that the emergence of multisite CPET, with hydronium ion as the proton donor, may prove a general feature of sufficiently endergonic reductions of dioxygen by otherwise "outer-sphere" complexes (or electrode reactions) at sufficiently low pH values in water.

Acknowledgment. I.A.W. thanks the Toman Foundation (Ben Gurion Univ.) and the ISF (248/09, 1667/09 and 1720/08) for support, C. Besson for analytical data, and J. Roth, C. Costentin, A. B. Anderson, D. Meyerstein, E. T. J. Nibbering, and E. Pines for valuable input. Y.W. thanks the Israeli Ministry of Education for a VATAT Post-Doctoral Fellowship.

Supporting Information Available: Absorbance versus time plots; electrochemical data; control experiments and kinetic data for reactions of $\mathbf{1}_{1e}$, $\mathbf{2}_{1e}$, $\mathbf{3}_{1e}$, and $\mathbf{4}_{1e}$; Eyring plots; calculations of activation parameters using the Marcus model (including the temperature dependence of $\Delta G°$); plot of k_{ET} and $k_{CPET}[H^+]$ as a function of average distances between O_2 and H^+; and additional discussion. This material is available free of charge via the Internet at http://pubs.acs.org.

JA104392K